EVALUATION OF ISOLATION DETAILS TO ENABLE ROCKING IN A MASONRY VENEER PANEL

By

LOUIS MARIE GOUHIER DE FONTENAY

A thesis submitted in partial fulfillment of
the requirements for the degree of

MASTER OF SCIENCE IN CIVIL ENGINEERING

WASHINGTON STATE UNIVERSITY
Department of Civil and Environmental Engineering

DECEMBER 2012

To the Faculty of Washington State University:

The members of the Committee appointed to examine the thesis of LOUIS MARIE GOUHIER DE FONTENAY find it satisfactory and recommend that it be accepted.

_____

David I. McLean, Ph.D. P.E., Chair

_____

James D. Dolan, Ph.D., P.E.

_____

William F. Cofer, Ph.D., P.E.

ACKNOWLEDGEMENTS

I would like to acknowledge the National Institute of Science and Technology for their financial support of this project. I also would like to recognize KPFF Consulting Engineers, and particularly Steve Dill of KPFF, for providing the impetus and structural details for the rocking panel.

I would like to express my deepest gratitude to Dr. David McLean for serving as my committee chair and for giving me the chance to work on this project. His patience, guidance, support and knowledge greatly helped me get through my master's program. I would also like to thank Dr. Dan Dolan and Dr. Bill Cofer for serving as members of my graduate committee. Their availability, kindness and advice are really appreciated.

I sincerely thank the people at the Composite Materials and Engineering Center, especially Bob Duncan, Scott Lewis, Kyle Spangenberg, Danny Mjelde and Tim Spry for their assistance in constructing and testing my specimens. In addition, I want to acknowledge Vicki Ruddick for her help with the administrative details associated with my graduate program. I also extend my thanks to Derek Ohlgren and Carl Harris for their help.

Finally, I would like to thank my family and friends for their support and love during this 18 month program, so far away from home.

EVALUATION OF SPECIAL DETAILS TO ENABLE ROCHING IN

A MASONRY VENEER PANEL

ABSTRACT

By Louis Marie Gouhier de Fontenay, M.S.
Washington State University
December 2012

Committee Chair: David I. McLean

The objective of this project was to evaluate the effectiveness of special isolation details designed to enable rocking response in masonry veneer panels subjected to lateral displacements. Rocking is expected to reduce or eliminate damage to the masonry panel in a seismic event. Criteria considered in evaluating the performance of the panels and isolation details included strength, energy dissipation, residual displacement, extent of damage and rocking behavior.

Two panel specimens were constructed and tested under quasi-static cyclic lateral loading and constant axial (vertical) loading. One panel had 20 kips of axial load, and the other had 50 kips, which was later reduced to 40 kips due to testing capacities. Special details were incorporated at the base of the panels to enable rocking. Two steel dowels were placed across the interface between the panel and footing. The dowels included a bond breaker such that only shear could be resisted by the dowels. In addition, the interface included a neoprene pad in the center region of the panel and two strips of compressible foam at the ends. The neoprene pad served to transmit axial loads and shear between the panel and the footing, and the foam strips protected the ends of the panels once rocking occurred.

Both panels exhibited rocking behavior. Very little damage occurred to the first panel with the lower axial loading. The second panel with the higher axial loading underwent a more

complex response mechanism and experienced substantial damage. The larger axial loads for Panel 2 also resulted in increased lateral capacity and stiffness. Yielding of the dowels contributed significantly to energy dissipation in the specimens. Friction and sliding of the panel on the neoprene pad was also a major contributor to energy dissipation.

For the panel with lower axial loading, only minor damage developed in the panel even when loaded to 3 in. of lateral displacement, corresponding to a lateral drift of more than 5%. Even in the panel with higher axial loading, significant damage did not develop until the lateral displacements exceeded 1.0 in of lateral displacement, corresponding to a lateral drift of nearly 2%. The special isolation details proposed for the veneer panels were successful in developing the intended rocking response.

TABLE OF CONTENT

Page

LIST OF TABLES

Page

LIST OF FIGURES

Page

CHAPTER 1: INTRODUCTION

1.1 Background

In many countries, a significant portion of residential and commercial buildings are constructed with masonry, including both structural masonry and masonry veneers. The use of masonry often reduces costs and construction time. Unreinforced masonry structures have traditionally performed poorly in seismic events due to limited ductility once their strengths are exceeded. In addition, unreinforced masonry may experience brittle shear failures. Because of this limited ductility, unreinforced masonry is no longer used in areas with significant seismic activity. Typical failure modes of masonry shear walls are depicted in Figure 1.1. It was with these modes in mind that researchers and engineers developed steel reinforced shear walls to make them capable of satisfactorily resisting an earthquake.

All modern structures, whether constructed of masonry, timber or reinforced concrete, are typically designed to behave in a ductile manner in order to dissipate energy and provide advance notice of distress. Designing to produce ductile response is the widely accepted philosophy for modern seismic design. Structures in seismic zones must incorporate special detailing to achieve the required ductility and thereby prevent collapse during an event and ensure the safety of its occupants. Ductility is achieved and energy is dissipated through inelastic deformations of the reinforcement in critical regions of the structures, referred to as plastic hinge zones. These inelastic deformations lead to permanent damage which will typically require repair after a large seismic event. However, such damage is acceptable in a major event, even if it means that the structure will need to be partially or even entirely rebuilt, but it must not collapse.

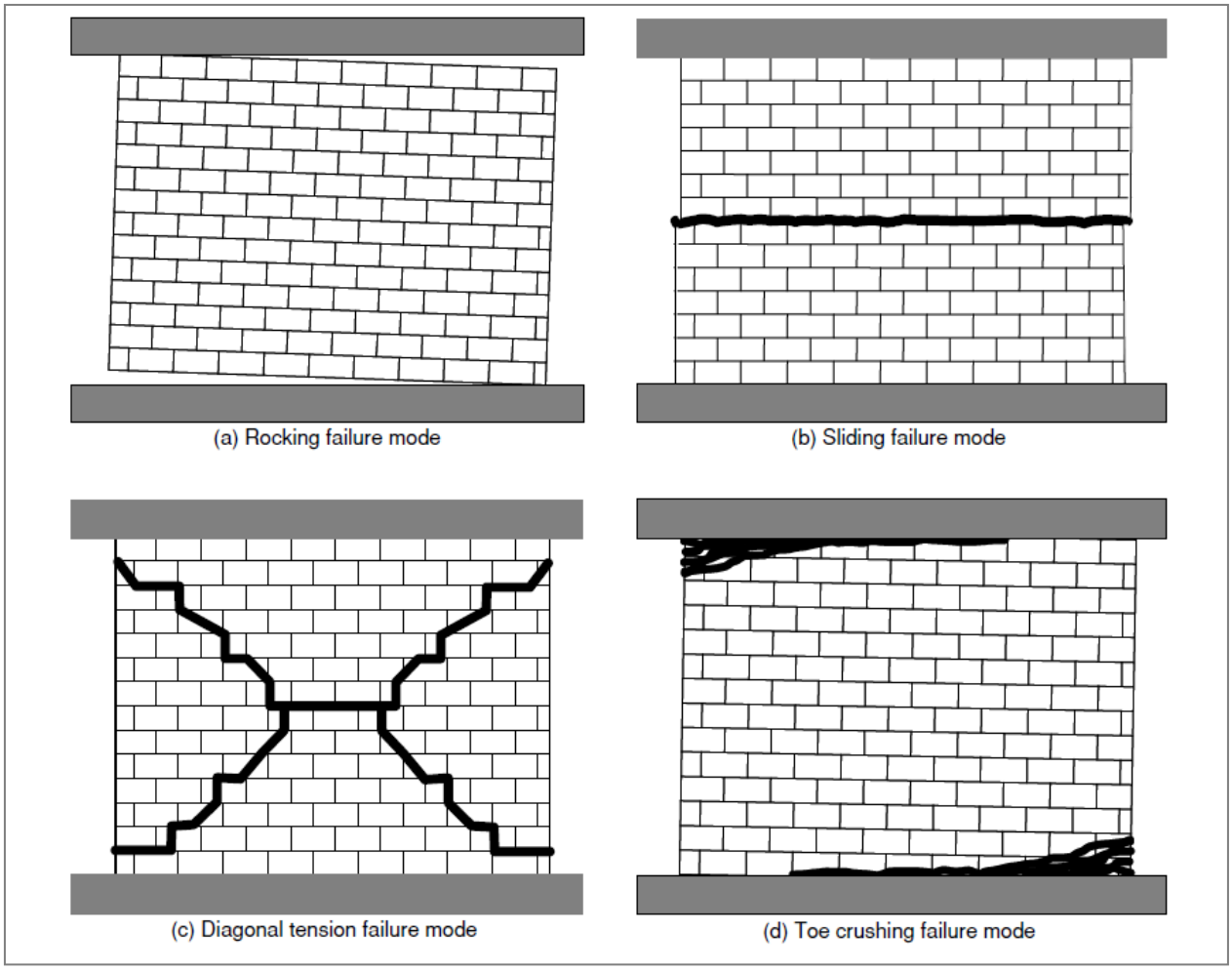

Figure 1.1: Failure Modes (from Lee, Li, Oh, Yang and Yi, 2008)

Performance-based design is a new design philosophy that is increasingly being used by structural engineers that seek to limit the extent of damage under one or more loading scenarios. Elastic design can be used so that structures always stay in the elastic range. However, elastic design is an uneconomical as well as an unnecessary design approach except for highly critical buildings such as nuclear power plants where damage may result in a significant hazard. The effects of the March 2011 magnitude 9.0 earthquake and subsequent tsunami on the Fukushima nuclear power plant represent an example of this hazard. To be economical, most buildings are designed for seismic loads using a Response Modification Factor, referred to as the R-factor,

which allows for a reduction in the elastic capacity by accounting for energy dissipation through plastic deformations.

An alternative solution to produce seismically resistant structures is seismic isolation. With this design approach, the energy of an event is dissipated through mechanical devices. Base isolation is one of the more common ways of protecting structures. By decoupling the building from the ground, base isolation can be utilized to protect it from the horizontal movements caused by an earthquake. For example, by mounting rubber bearings between the building and its foundation, little or no ground movements are transmitted into the structure itself. The system not only provides protection to the building but also to its contents and occupants. Nevertheless, it does not make the building seismic-proof as often times the building will still be damaged during critical events. This type of isolation system also typically adds to the cost of a building.

Another structural isolation method utilizes a rocking response of the building. Rocking systems were among the first isolation systems and allow for a building to rock on its base to enable the building to survive major earthquakes with little or no damage, provided that the building does not lose its stability and overturn during the shaking. Surprisingly, with such promising potential, these systems have not been widely utilized in practice. With increasing demand for improved seismic performance, the interest in rocking systems has increased in the last two decades. However, research in and applications of rocking systems still lag behind other alternatives for isolation systems.

1.2 Scope and Objectives

This project was initiated through discussions with KPFF Consulting Engineers based on isolation details designed to enable rocking in masonry veneer panels in high-rise structures.

Steve Dill of KPFF served as the primary contact for information on the proposed system. The research was conducted at Washington State University. The objective of the project is to investigate the effectiveness of the isolation details to enable rocking response in a masonry veneer panel subjected to lateral displacements. Rocking is expected to reduce or eliminate damage to the masonry panel in a seismic event. Two panel specimens with the same rocking details and geometry were subjected to cyclic, quasi-static lateral loading under different axial loadings. Criteria considered in evaluating the performance of the panels and isolation details included strength, energy dissipation, residual displacement, extent of damage and rocking behavior.

CHAPTER 2: LITERATURE REVIEW

2.1 Introduction

There are a limited number of modern structures that have been designed to enable rocking on their foundations. Provisions addressing rocking mechanisms as a seismic isolation system are not yet included in current US building codes. Nevertheless, interest in rocking systems has risen recently as another option for seismic isolation of structures.

This chapter includes a general discussion of the rocking mechanism, summaries of several experimental and analytical studies that have contributed to a better understanding of rocking in structures, and a review of rocking provisions in building codes from around the world.

2.2 Rocking Mechanism

A rocking wall is a non-linear elastic system that exhibits a response that can generally be classified as bilinear. The wall first behaves as a fixed-base wall before the rocking mechanism starts. The rocking mechanism stops when the neutral axis migrates close to the wall edges, triggering overturning of the wall. Assurance has to be made in the design that the wall does not overturn.

One of the biggest issues that must be addressed with rocking systems is that the dissipation of energy is negligible compared to systems designed to behave ductily (Holden, Restrepo and Mander, 2002). Rocking of the structure also leads to significantly higher lateral displacements with little increase in lateral loads (due to rigid body behavior), whereas ductile design is the opposite (high lateral forces and small displacements). In general, standard masonry buildings are typically too stiff to activate a rocking mechanism. If rocking does happen, it is considered as a

failure mode. Figure 2.1 displays the expected load-displacement curve of a laterally-loaded rocking wall under a unidirectional push. This figure does not account for a damping system, a self-centering system, or damage to the edges (toes) of the wall.

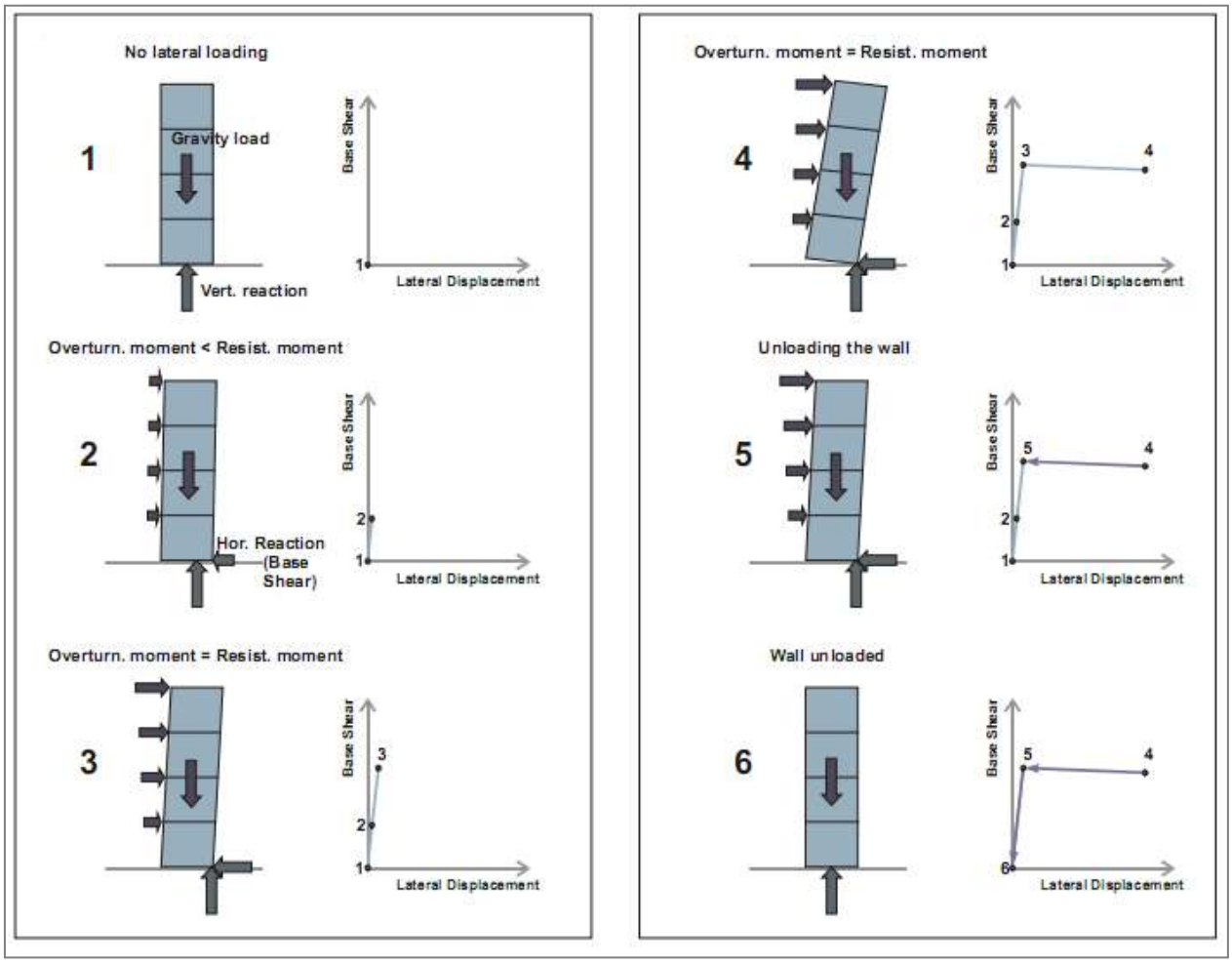

Figure 2.1: Lateral Static Loading of a Rocking Wall (from Toranzo, 2002)

2.3 Self-centering Issue

Self-centering is the ability of a structure to come back to its initial position by itself. In the case of a wall, this would mean that the wall comes back to vertical and that no residual sliding is present at the base.

The self-centering of a wall after the rocking event is an important issue (Christopoulos, Filiatrault and Folz, 2002). Excessive residual deformations can lead to the destruction of the structure, even days after a seismic event.

Figure 2.2 shows an idealized force-displacement response of a linear elastic system and the response of a yielding structure (i.e., using ductile design). As a large fraction of the energy is dissipated through hysteretic response, significant residual displacements may be present. The system can dissipate significant energy (area enclosed by the curves), but no self-centering can be expected because of plastic deformations.

In contrast, self-centering system shows a characteristic flag-shaped hysteresis curve (see Figure 2.3). The amount of dissipated energy may be significantly reduced, but the system returns to its original position (no residual drift).

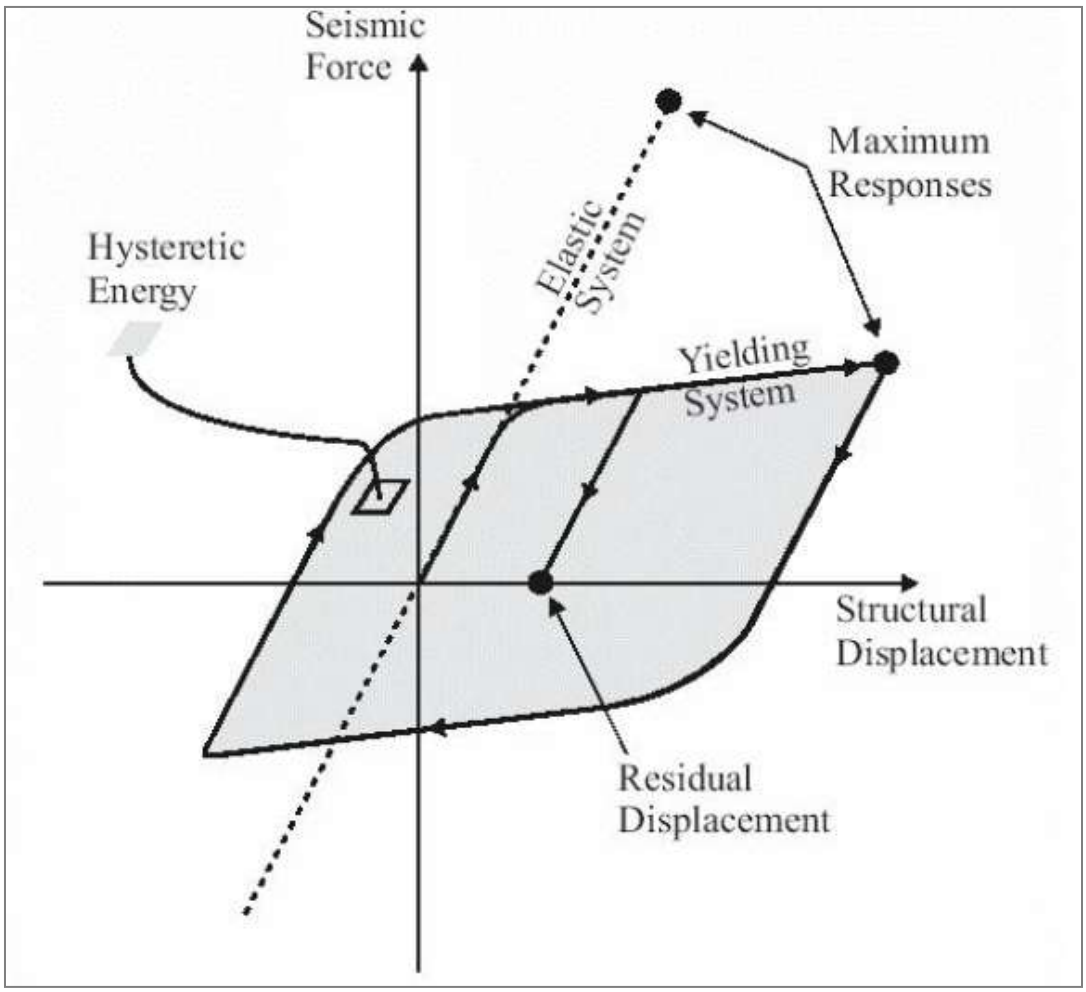

Figure 2.2: Idealized Seismic Response of Yielding Structure (from Christopoulos et al. 2002)

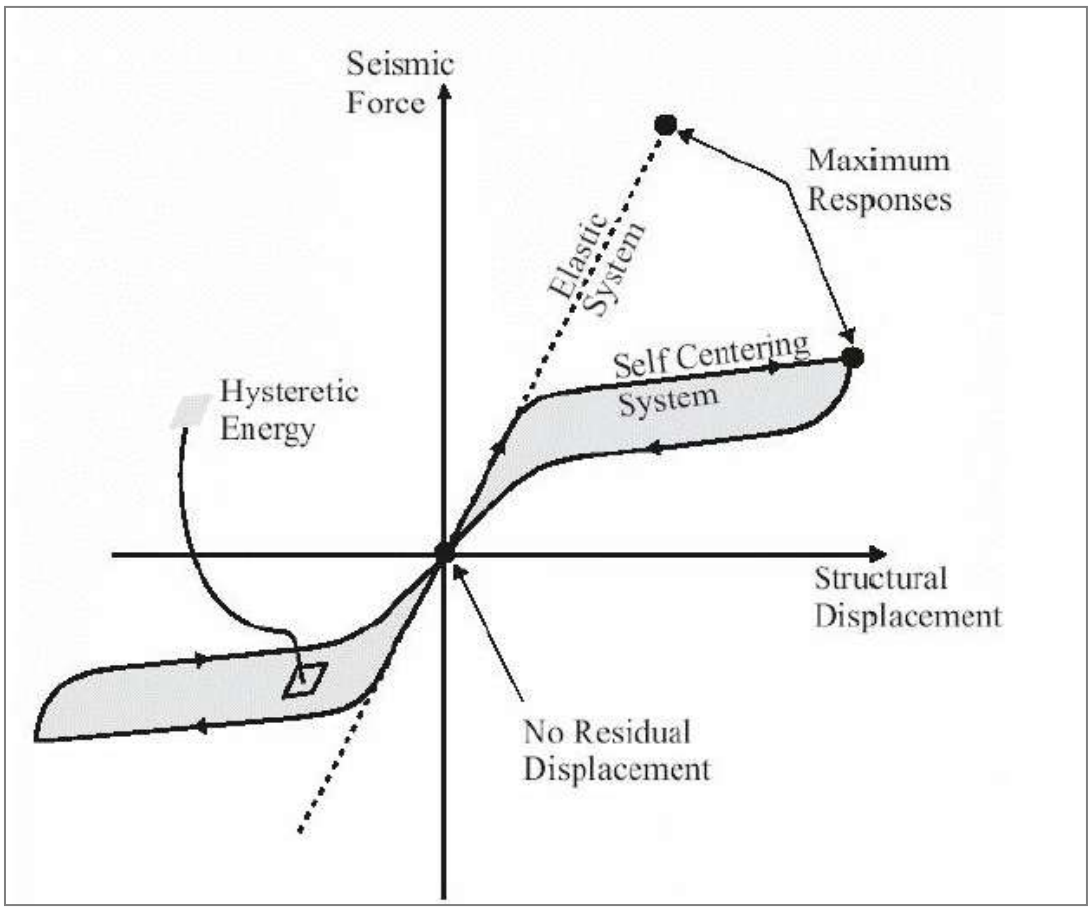

Figure 2.3: Idealized Seismic Response of Rocking Structure (from Christopoulos et al. 2002)

The concept of self-centering systems was proposed by Stanton et al. (1997) and was extended by Restrepo (2002) to reinforced concrete cantilever walls by using a hybrid jointed wall, by Shen (2000) to concrete coupled walls, and by Kuruma (2004) to cantilever walls with vertical joints. The proposed systems all incorporated post-tensioned axial tendons within the structures. The results were promising with no residual displacements observed.

Prestressed tendons provide axial load (depending on the prestressing force) and self-centering properties. The tendons were used in recent research (Filiatrault, Restrepo and Christopoulos, 2004) as part of a larger study investigating precast concrete moment-resisting frames and interconnected shear walls under the US PRESSS program (PREcast Seismic

Structural System) directed by Priestley until 1999. Results from the PRESSS program proved to be effective and are now incorporated in a number of building codes for specific types of structures.

2.4 Code Provisions

Neither the US building codes nor the European building codes include any provisions accounting for rocking mechanism as the basis of the design. Only the New Zealand building code specifies some details accounting for rocking in design. Brief discussion is given for each of these codes in the following sections.

2.4.1 US Codes

As noted earlier, the US building codes do not provide any guidelines to base the design of structures on a rocking mechanism. FEMA 306 (1998) does provide an equation (Equation 1-4) for evaluating the amount of strength for sliding or rocking in the design, but it does not recommend rocking as a desired system. In addition, FEMA 356 (2000) provides a procedure to account for rocking behavior by calculation of the amplitude of rocking. The procedure involves the following steps:

- Calculation of the mass, weight, and center of gravity for the rocking system (or subsystem);
- Calculation of the soil contact area, center of contact, and rocking system dimension, R;
- Determination of whether rocking will initiate;
- Calculation of the effective viscous damping of the rocking system (and the corresponding design displacement spectrum); and

- Calculation (graphically or iteratively) of the period and amplitude of rocking (the solution will not converge if overturning will occur).

Although rocking provisions have not yet been implemented in US building codes, some particular innovative types of ductile connections like the *jointed ductile connections* or *hybrid systems* have been tested and are currently being approved by US committees. Guidelines for the design of such structures should be available for design soon. See ACI T1.2-0.3 (2003) for more information about such systems. However, according to the US building codes, new design methods can be used if a special study is performed. See for example the *Building Code Requirements and Specification for Masonry Structures* (MSJC, 2011), article 1.3.

2.4.2 European Code

In Europe, *Eurocode 8 - Design of Structures for Earthquake Resistance* (EN 8, 2008) accounts for rocking or sliding in certain structural components such as large, lightly-reinforced walls (Section 1.4). These options are taken into account with the use of a q-factor, referred to as the behavior factor. The code recognizes the stable nonlinear-elastic behavior that can result from rocking, but it judges that it is difficult to address this type of behavior in design (Section 5.1.2). Consequently, no procedures are given except for, like the US code, some specific, deeply studied solutions such as for jointed ductile connections.

2.4.3 New Zealand Code

In contrast to US and European codes, the New Zealand building code (NZS 4203: 1976) has incorporated rocking mechanisms in its design provisions for quite a long time.

In 1981, New Zealand constructed a state-of-the-practice bridge incorporating rocking: the South Rangitikei Railway Bridge. Each column footing of this 315-m (1033-ft) long bridge was equipped with torsional beam mechanical energy dissipating devices. These devices were designed to allow slight rocking on the foundations.

Where dissipation of energy is through rocking of the foundations, the New Zealand code requires that the structure shall be subjected to a special study, except that this need not apply if the structural ductility factor is equal to or less than 2.0. These restrictions led designers to design many low-rise shear wall buildings governed by rocking mechanisms (Priestley, Evison and Carr 1978).

Subsequently, NZS 1170.5:2004 replaced NZS 4203 and required that a special study be performed when rocking is implemented as a method of seismic isolation with energy dissipation during seismic excitation. This special study should entail the development of a computer model and a time history analysis of the structure. However, most design offices cannot provide this type of advanced analysis and, consequently, the cost of this analysis is only justified for the large structures. Following these new requirements, researchers are currently developing guidelines for designers wishing to use rocking elements (Kelly, 2009).

2.5 Historical Review of the Interest in Rocking Systems

Housner (1963) was the first to find that the rocking mechanism could be a seismic solution. He observed that, despite some apparent instability, several golf-ball-on-a-tee types of elevated water tanks survived the ground shaking motion of the 1960 Chilean earthquake. In contrast, some significantly stiffer structures were completely destroyed. Following this observation, Housner analyzed the free oscillations of a rocking block (rocking period, energy

loss, overturning acceleration, etc.) and showed that the stability of a tall slender block subjected to earthquake motion is much greater than its stability with constant horizontal force. Additionally, the rocking behavior mode makes the wall act as a rigid body (Aslam et al, 1980).

It was not until 1978 when Meek (1978) introduced aspects of structural flexibility coupled with rocking structures that the interest in the rocking mechanism was subjected to more research. Aslam et al. (1980) analyzed the rocking and overturning response of massive concrete blocks with a high aspect ratio. They considered, among other things, the influence of prestressing. Prestressing provided additional lateral resistance, anchored the structure to the footing and gave an improved rocking resistance. In particular, it prevented excessive rocking.

Priestley and Tao (1993) proposed a new beam-to-column connection. The beams were designed and constructed so that they could rock at the column interface. They used partially unbound tendons (following Aslam's results) and used special spiral confinement in the beam plastic hinge regions. The idea was to prevent damage in the connections by limiting the energy absorbed during large lateral displacements. They observed that damage still occurred in high-force regions such as the rocking toe. The use of tendons was also investigated for beam-column connections (Garcia-Pujador, 1998), (Cheng, 2008), (Roh and Reinhorn, 2010), walls: (Pennucci et al., 2009), (Kuruma, et al., 1999) (Hitaka and Sakino, 2008) (L. Toranzo, 2002) (Restrepo and Rahman, 2007) and frames (Stanton et al., 1997) (Christopoulos et al., 2002).

A new philosophy for rocking was developed by Mander and Cheng (1997) and was referred to as Damage Avoidance Design (DAD). As the name implies, DAD attempts to prevent significant structural damage during an event, enabling the continued use and operation of the building following the event. While some damage might be unavoidable, this philosophy would attempt to limit both the time and monetary costs of any necessary repairs.

2.6 Previous Research

2.6.1 Rocking Behavior of Rigid Objects (Prieto and Lourenço, 2005)

Equations developed by Housner to describe rocking response (Housner, 1963) have been periodically improved, adjusted and corrected. Lipscombe (1990) proved experimentally that Housner's equations were not accurate for blocks with an aspect ratio smaller than 4. An optimized formulation was proposed by Prieto and Lourenço (2005) to solve two important drawbacks: the complexity and the intractability for a generalization with a high number of blocks. Equations are provided in this reference for defining the rocking mechanism of rigid blocks.

2.6.2 Seismic Performance of Precast Reinforced and Prestressed Concrete Walls (Holden, Restrepo and Mander, 2002)

Following their previous project, Holden et al. (2002) investigated the performance of two precast concrete cantilever wall units. Precast walls are becoming more common for their cost efficiency, and they also allow quicker installation and high quality control. The main disadvantages of precast walls are that regions resisting lateral forces are likely to undergo heavy damage in moderate seismic events. Precast panels require special detailing such as the continuity of vertical reinforcement passing through areas where plastic deformations are expected.

The first specimen was designed according to the New Zealand code (SNZ 1995) as a reinforced specimen reacting in a ductile manner, whereas the second incorporated a partially prestressed system and was able to rock on its foundations. Table 2.1 summarizes the differences.

Note that the two walls were built with the same geometry and the same concrete material. Figure 2.4 shows the lateral force-displacement response obtained from testing of the two specimens.

The code-compliant specimen was heavily damaged, whereas the second specimen had no visible damage. Even for a small drift (lateral displacement/height), the damage for the first specimen was extensive. The first system dissipated more energy but showed significant residual deformation, whereas the rocking specimen maintained self-centering characteristics. They concluded that the hybrid specimen had significant positive qualities and required deeper investigation.

Table 2.1: Comparison between Ductile and Hybrid Walls (adapted from Holden et al., 2002)

System Property	Monolithic	Hybrid
Energy Dissipation Capacity	Excellent	Good
Special Reinforcing Detailing	In potential plastic hinge zones	Only required at wall ends and foundation beam where rocking takes place
Dimensional Limitation	To prevent plastic hinge instability	Minimum - based on elastic theory as wall panels remain essentially crack-free
Minimum Reinforcement Requirements	Can significantly increase the moment capacity at the critical region	Temperature and shrinkgage can be substituted with fiber reinforced concrete
Expected Postearthquake Repair Work	In plastic hinge zones, repair work can vary from epoxy injection to concrete replacement. Bars instability could also requires demolition. Permanent deformation	None expected, self-centering, no permanent deflections
Initial Cost	Competitive- widely used systems	Competitive? Requires cost analysis
Life-cycle Cost	Competitive relative to other conventional systems. Postearthquake repair may be required	Expected to be very competitive, no postearthquake repair needed

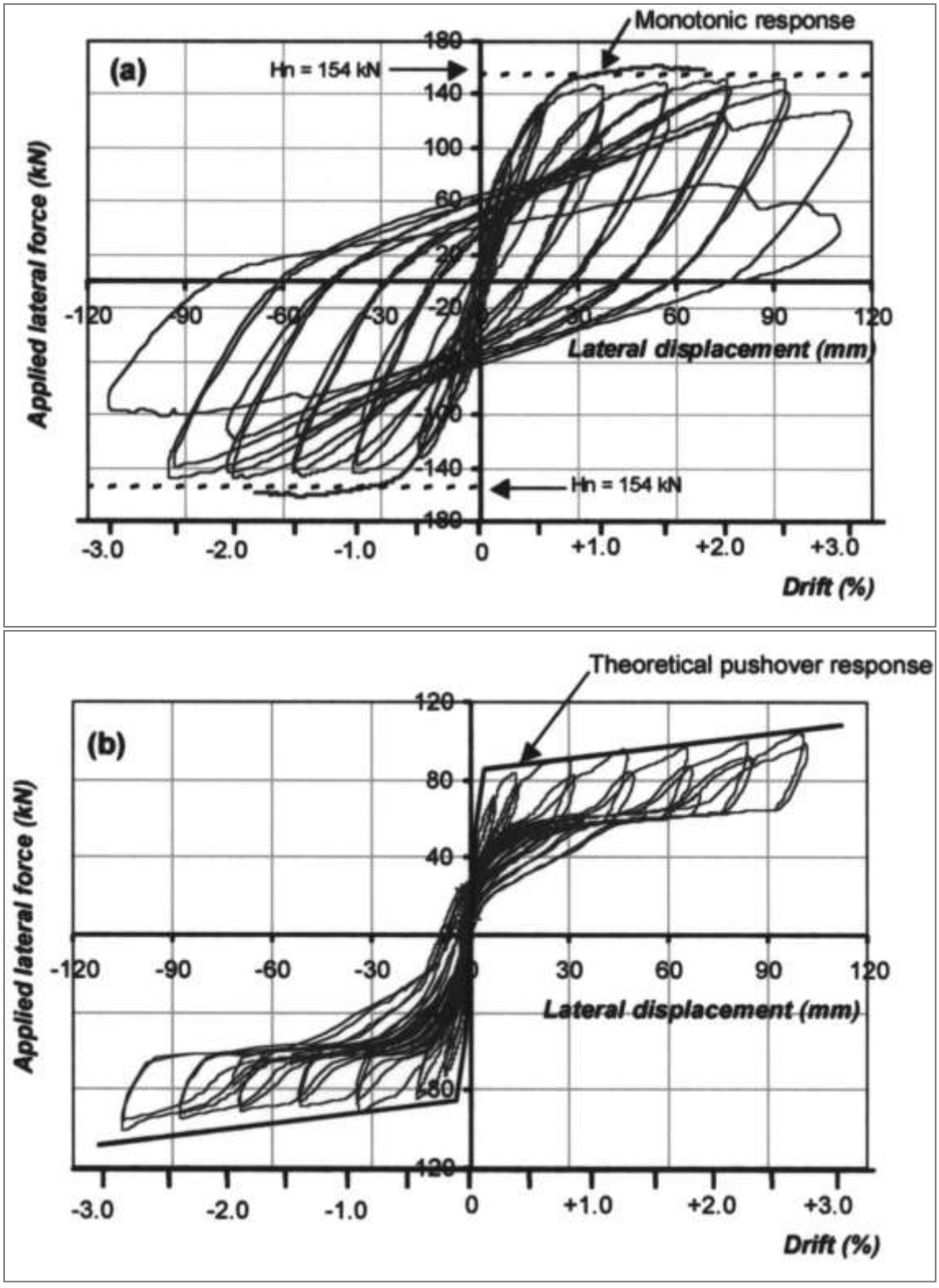

Figure 2.4: Load-Displacement Curves of Ductile and Hybrid Walls (from Holden et al., 2002)

2.6.3 Shake-Table Tests of Confined-Masonry Rocking Walls with Supplementary Hysteretic Damping (Toranzo, et al., 2009)

Toranzo et al. (2009) conducted tests to validate the concept of rocking walls as a major seismic system. They specifically tested confined masonry walls, but their findings can also be used with other kinds of rocking wall systems.

Confined masonry is a widely used method that consists of unreinforced brick panels surrounded by reinforced concrete elements (beams and columns). A typical confined-masonry specimen is shown in Figure 2.5. The concept of controlled rocking is an economic option for common low-rise buildings built with confined masonry.

Toranzo et al. used a 0.4-scale model frame wall incorporating steel hysteretic energy dissipating dampers referred to as EDDs. These devices were designed to meet the energy dissipation requirements while being easy to replace or fix. They recommended that the EDDs be placed at the toes of the rocking walls in order to dissipate energy through flexure. In addition, the EDDs need to be designed to transfer shear loads into the foundation. While these devices were deemed effective, Toranzo et al. recommended that supplemental damping be introduced to increase the damping.

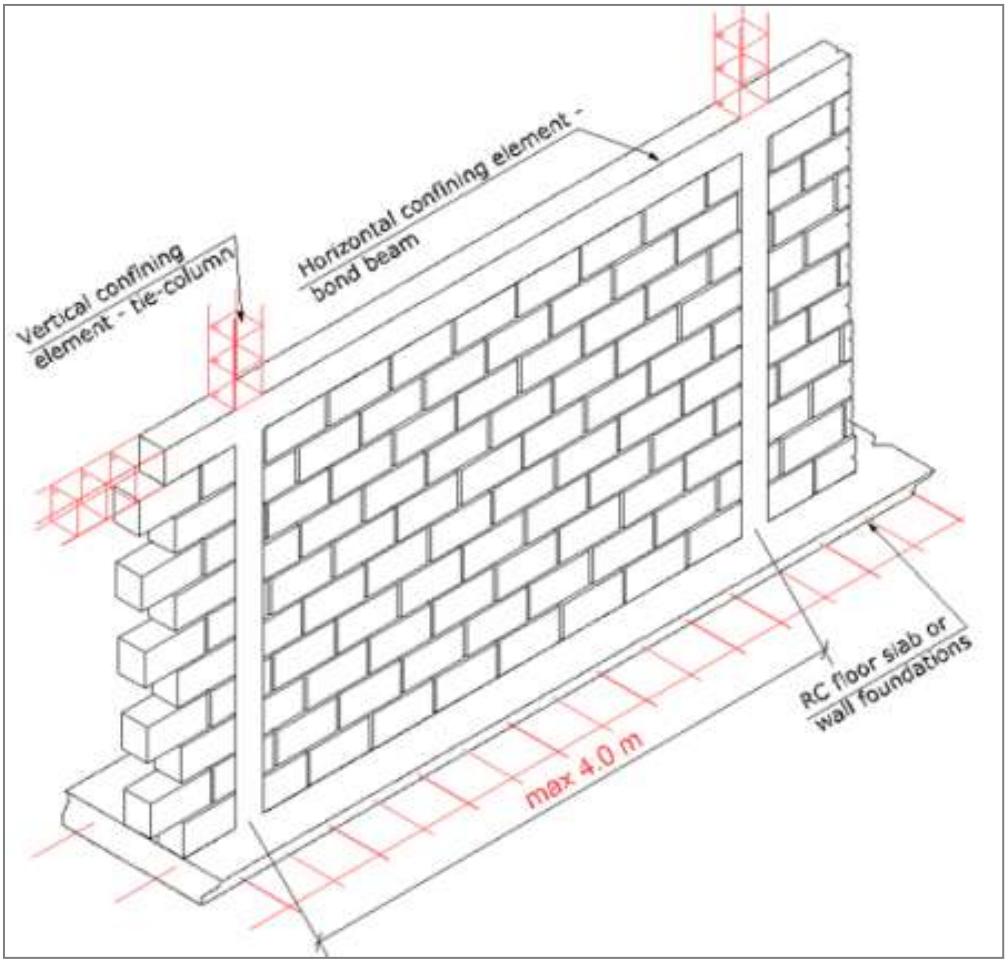

Figure 2.5: Geometry of the Wall (from Toranzo et al., 2009)

The setup of the test conducted by Toranzo et al. is shown in Figure 2.6. It was built to represent a typical three-story building commonly found in South America. It can be related to the research reported in this paper because the frame provides lateral bracing and the masonry is not fixed to the footing. They measured their displacement with an adaptation of the design methodology of Priestley (2000). Given the expected large stresses at the toes of the walls, they provide a 10-mm (3/8-in.) thick steel plate to avoid damage to the foundation as well a steel case to protect the corners of the wall from crushing. They concluded that, with careful and logical

detailing, damage can be eliminated and the wall returns to its original position providing no residual displacement.

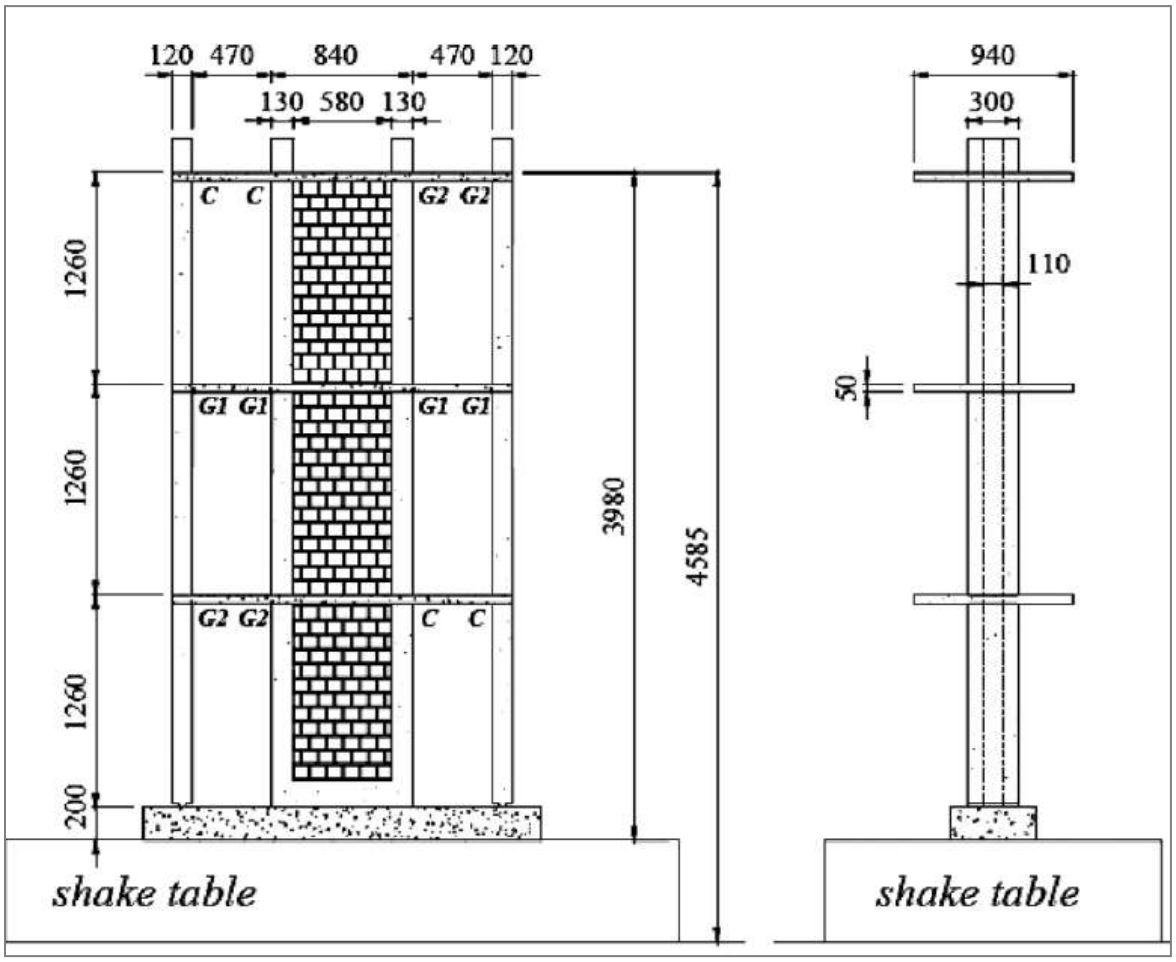

Figure 2.6: General Dimensions of the Test Structure (from Toranzo et al., 2009)

2.6.4 In-plane Experimental Behavior of Stone Masonry Walls under Cyclic Loading (Vasconcelos and Lourenço, 2009)

Vasconcelos and Lourenço (2009) studied the behavior of stone masonry walls, a traditional building material throughout history. As few experimental investigations of stone masonry are available in the literature (most are for concrete, steel or masonry building materials), they tested 23 walls in quasi-static loading. They simulated distinct types of walls

existing in ancient buildings of Europe under different loading modes. They tested different bond arrangements and many of these walls failed due to the rocking mechanism as can be seen in Figure 2.7. They stressed that, when only rocking of the wall occurs, global collapse does not occur. However, residual inelastic horizontal displacements were observed due to sliding along the bed joints of the units.

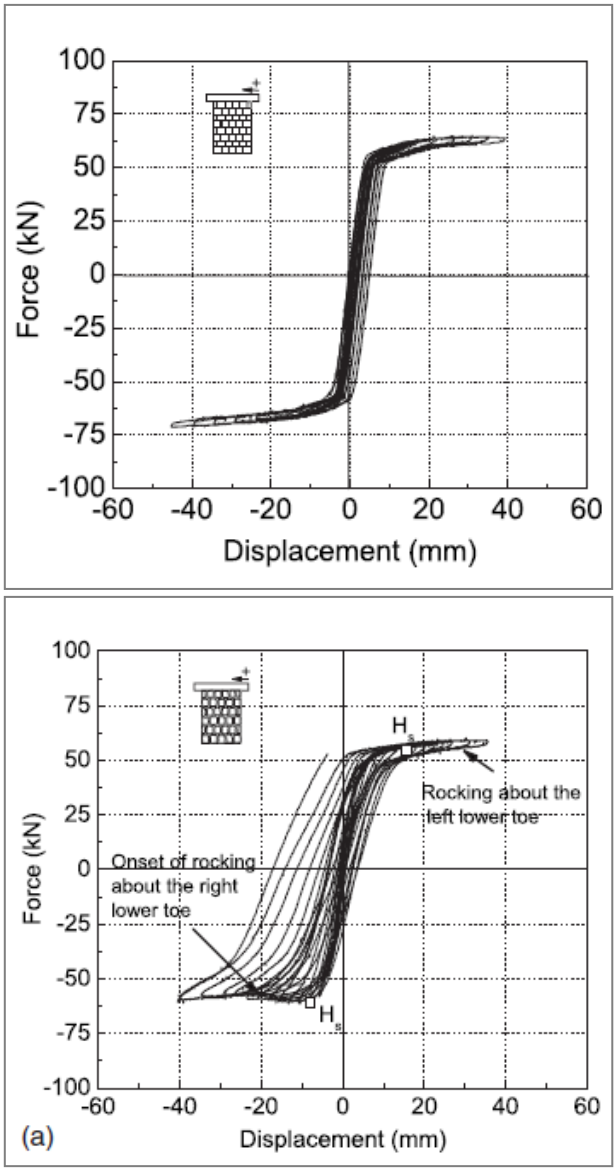

Figure 2.7: Rocking Hysteresis Curves for 2 Different Arrangements (from Vasconcelos and Lourenço, 2009)

In addition they noted that, in a real earthquake event, different effects can be amplified due to in-plane and out-of plane forces acting together. They concluded that, like masonry structures, the failure mode clearly depends on the level of axial load as well as the height-to-length ratio. They also found that the prediction of the lateral resistance through simplified methods agreed reasonably with the results from the experiments. A final conclusion from their study is that very little energy was dissipated unless some damage was done to the specimens. With the exception of the material used and the isolation details, these tests were very similar to those investigated in the masonry panels of this project.

2.6.5 Effects of Interface Material on the Performance of Free Rocking Blocks (ElGawady et al., 2011)

This research was conducted on the interface of free rocking blocks. Two types of test specimens were tested utilizing different properties such as the aspect ratio and the material at the interface. By doing this, the effects of the varying properties on the behavior of the blocks could be examined. The basic setup of these experiments is presented in Figure 2.8.

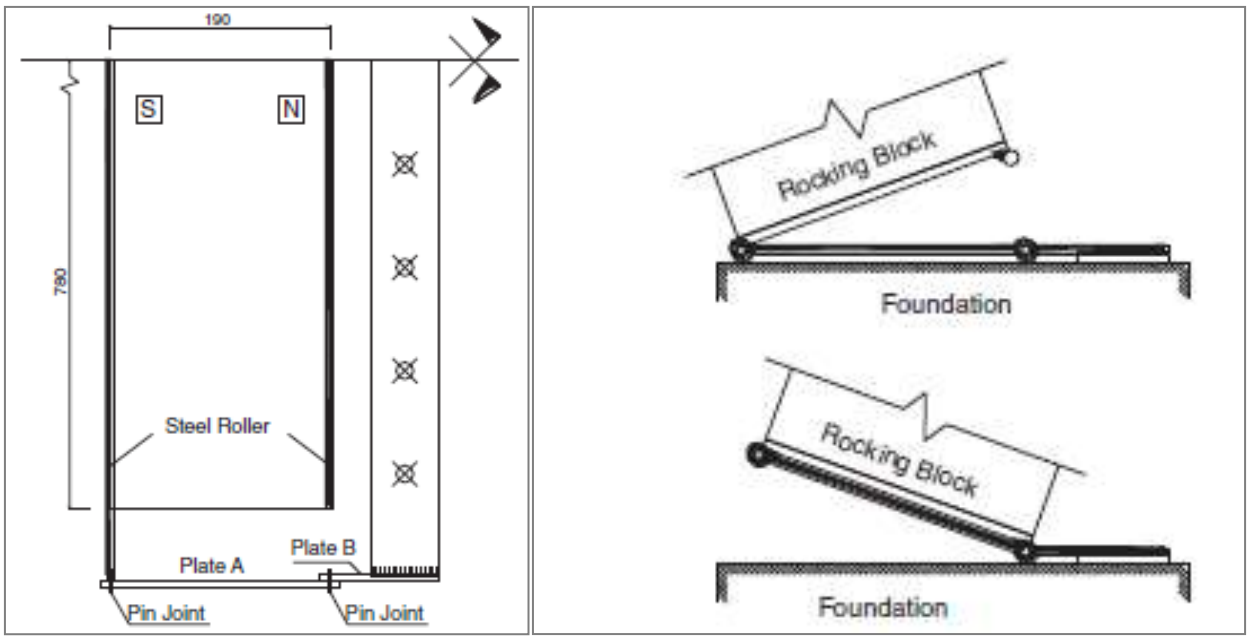

Figure 2.8: Plane View of the Specimen and Schematic of Rocking Mechanism (from ElGawady et al, 2011)

The paramaters investigated by ElGawady et al. included rocking period, rocking amplitude, and energy dissipation. They also attempted to compare the experimental results to the returns of existing rocking models. They reached the following conclusions:

- "Rocking response is very sensitive to any source of friction within or associated with the rocking system, either on or in the test specimen or its interface, as well as any small imperfections existing either in the specimens or the surface where the experiments were performed i.e. either the laboratory strong floor or the shaking table platform.
- The results of free rocking tests were repeatable. The test became more uniform with higher amplitudes and for tests on rigid foundations. For small amplitudes and for tests on rubber bases, the tests were still repeatable but with higher scatter."

Finally, they were able to predict the free rocking amplitude quite accurately when a coefficient of restitution was used.

CHAPTER 3: EXPERIMENTAL PROGRAM

3.1 Introduction

Two masonry veneer panel specimens were constructed to evaluate the performance of isolation details designed to enable rocking of the panels in a seismic event. The veneer panels are part of the building envelope and are not intended to resist lateral forces.

This chapter provides details of the two panel specimens, how they were constructed, and the procedures used to test the panels.

3.2 Footing description

The veneer panels were built on heavily-reinforced concrete footings. These footings already existed (from Sherman, 2011) and were reused in this project for the purpose of saving time as well as money. Some modifications were made to accommodate the details of the panel specimens. The footings were 24 in. wide, 18 in. deep and had a length of 86 in. Exact reinforcement in the footings is unknown, but these footings were designed for a much higher load resistance than that expected for this study (at least 10 times). The footings were then anchored in the laboratory floor with threaded rods to ensure the immobility of the footings during testing.

3.3 Panel specimen Description

The test specimen was designed and constructed to replicate the dimensions, details and support conditions of a rocking masonry panel developed by KPFF Consulting Engineers in Seattle. Drawings of the rocking masonry panel were provided by Steve Dill of KPFF. Details of

the rocking panel are presented in Figures 3.1 and 3.2. The masonry panel incorporates details at the top and bottom of the panel intended to enable rocking behavior and thereby reduce the damage that might occur from lateral displacements of the building system.

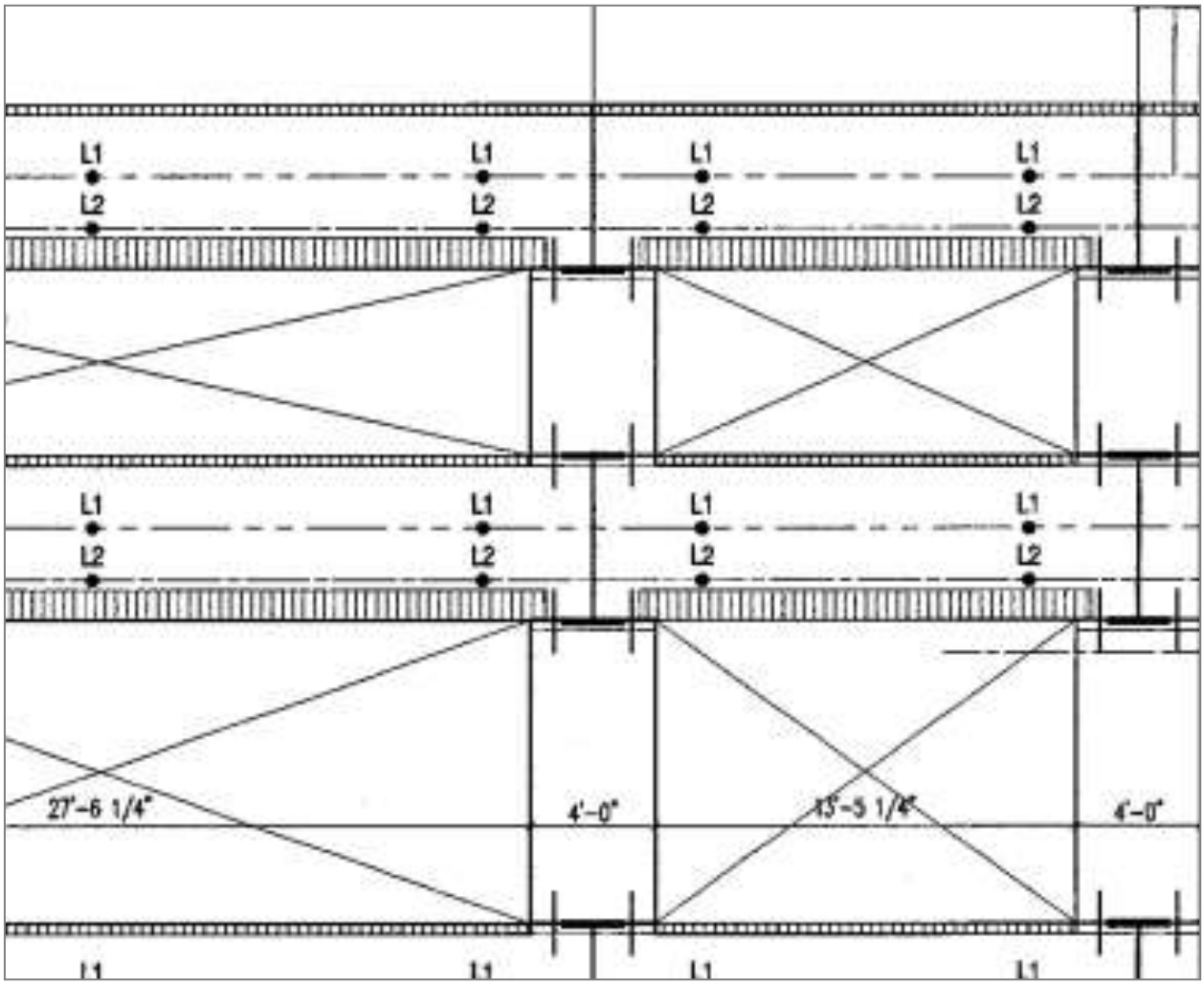

Figure 3.1: Building Drawing with Rocking Panel between Floors (from KPFF- Consulting Engineers)

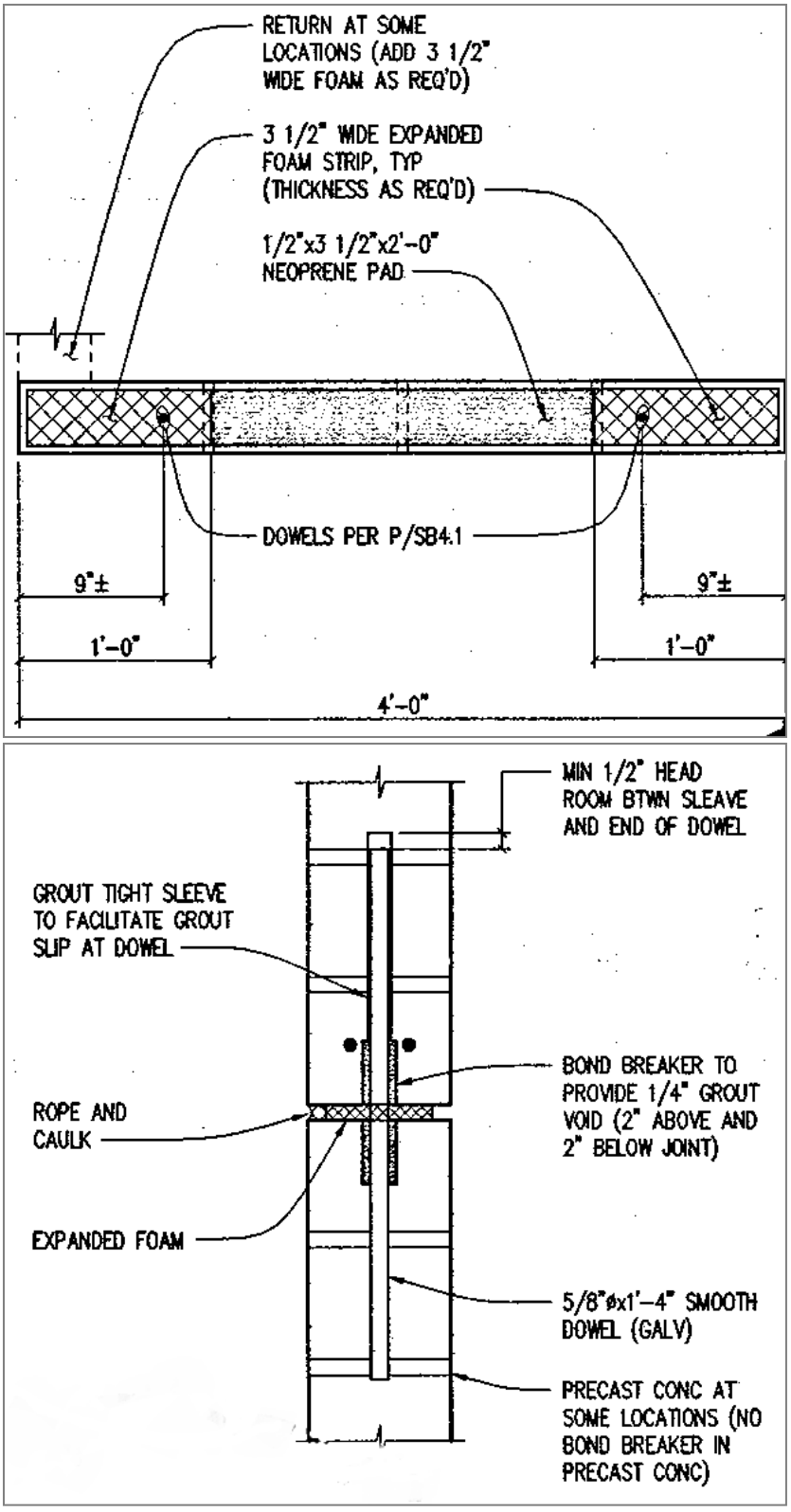

Figure 3.2: Panel Rocking Details (from KPFF- Consulting Engineers)

The test specimens were designed to represent half of the actual height of the masonry panel and incorporated the rocking detail only at the base. The specimens were free at the top, thereby effectively creating a cantilever condition for the panels. Nominal vertical and horizontal reinforcement was provided in the panels. The panels were first constructed on top of the heavily-reinforced footings, and reinforced loading beams were then constructed at the top of the panels. In accordance with the details provided by KPFF, the panel-footing interface incorporated a neoprene pad and foam strips as well as two steel dowels. Details of the test specimens are given in Figure 3.3.

The two panels were identical except for the material used in the foam strips. The two foam materials have similar compression resistance but different textures and internal structures. The neoprene pad is intended to provide transfer of axial loading and to resist shear sliding. It also acts to smooth out the interface, preventing any concentration of stress due to unevenness inherent in construction. The foam strips create a void at the bottom edges of the panel and are intended to reduce toe crushing. The bond breaker around the dowels, consisting of 4-in. long foam pipe insulation, provides a 0.25-in. void between the grout and the dowels. The neoprene pad and foam strips were purchased from Gardico Incorporated. Properties of the neoprene pad and foam strips are shown in Table 3.1. Note that CCNS stands for Closed Cell Neoprene Sponge.

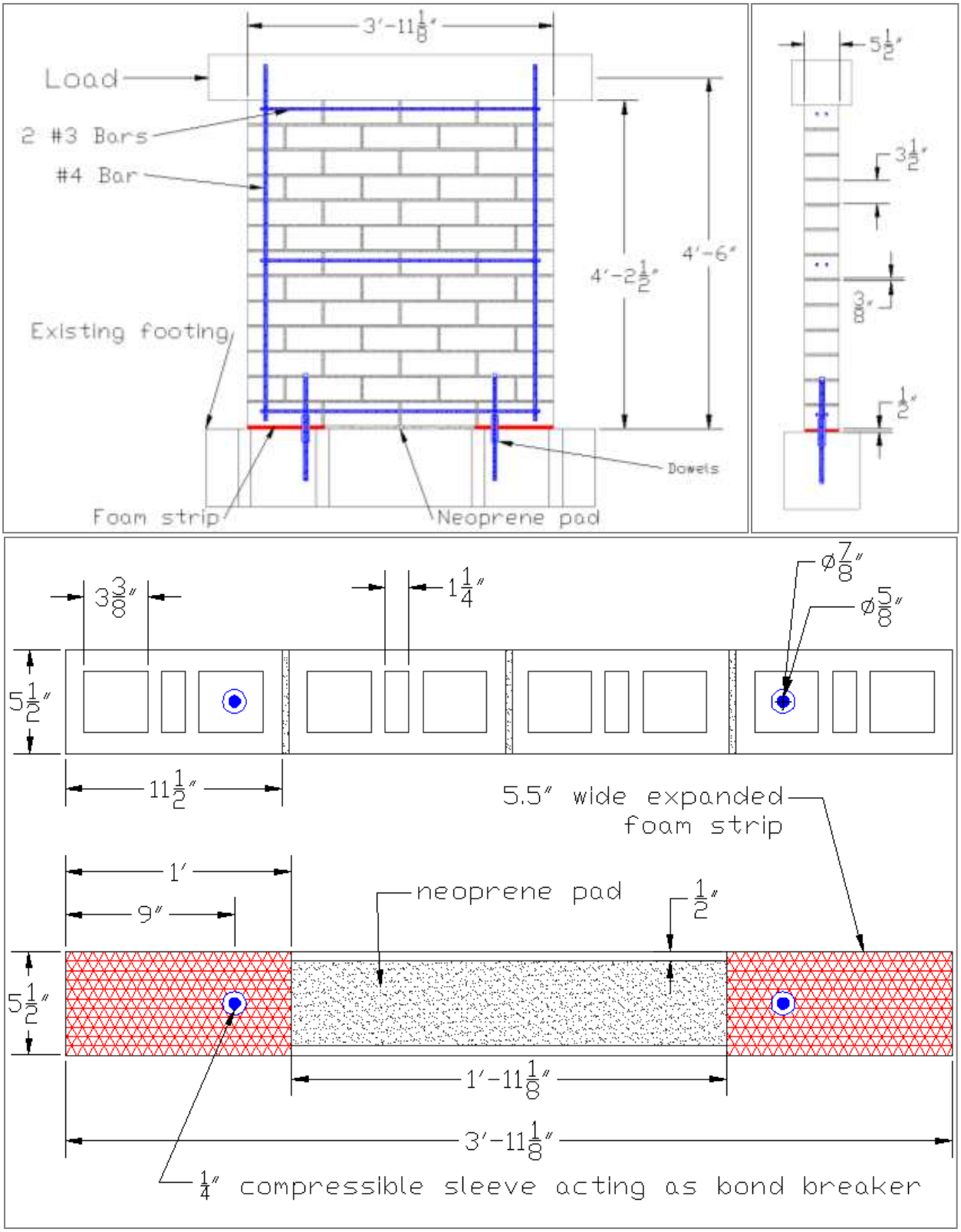

Figure 3.3: Panel Details

Table 3.1: Material Properties

	Neoprene	Foam
Panel 1	0.5 in. 60A Neo 60 Durometer	0.5 in. Styrofoam Expanded polystyrene
Panel 2	0.5 in. 60A Neo 60 Durometer	0.5 in. CCNS med density

A bond breaker was incorporated over the top half of the dowels to allow vertical slip between the dowels and the panel to enable rocking. The dowels also help to re-center the panel after rocking and, at large lateral displacements, resist shear and provide an energy dissipating mechanism once dowel yielding occurs.

3.4 Load Beam Description

Reinforced concrete beams were built on top of the two panels for use in applying the lateral load to the specimens. Each beam was 9.5-in. wide, 7-in. high and 60-in. long. Details are provided in Figure 3.4. Stirrups made from 0.25-in. diameter steel wire were used and spaced evenly at 6 in. throughout the length of the beam. The connection of the beam to the panel consisted of two different types of reinforcement. First, on the outer edges of the panel, vertical reinforcement extended from the bottom of the panel into the loading beam. Additionally, two hooks were grouted 5 in. into the top row of bricks cells and then extended 5 in. into the load beam.

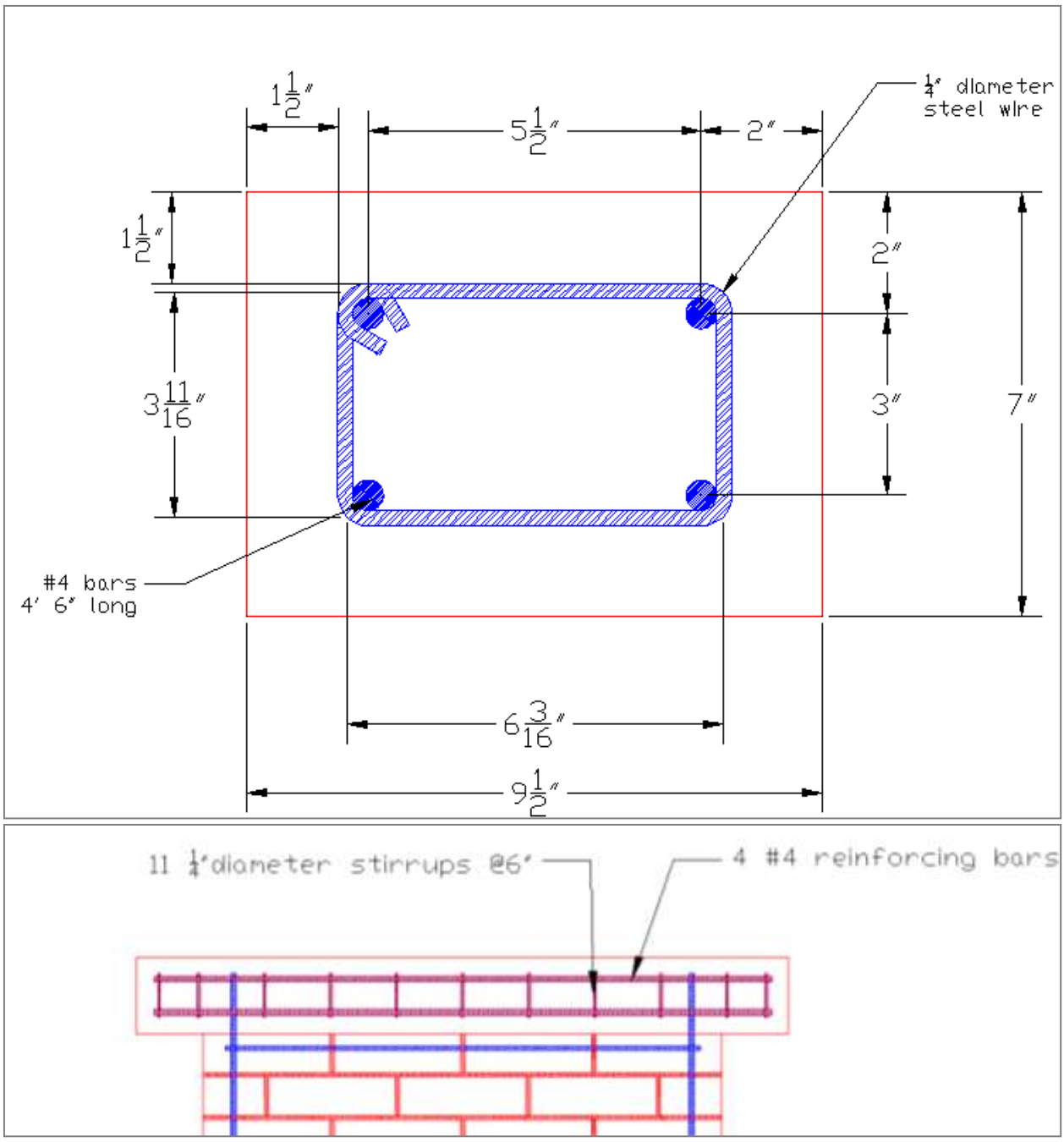

Figure 3.4: Loading Beam Details

3.5 Material Properties

The panel specimens were constructed using structural clay bricks provided by Mutual Materials in Seattle. The bricks used were 6 in. stretcher structural bricks. Bond beam bricks with

same dimensions were used to at locations with longitudinal reinforcement. The nominal dimensions of the masonry blocks were 6x4x12 in. See Figure 3.5 for details.

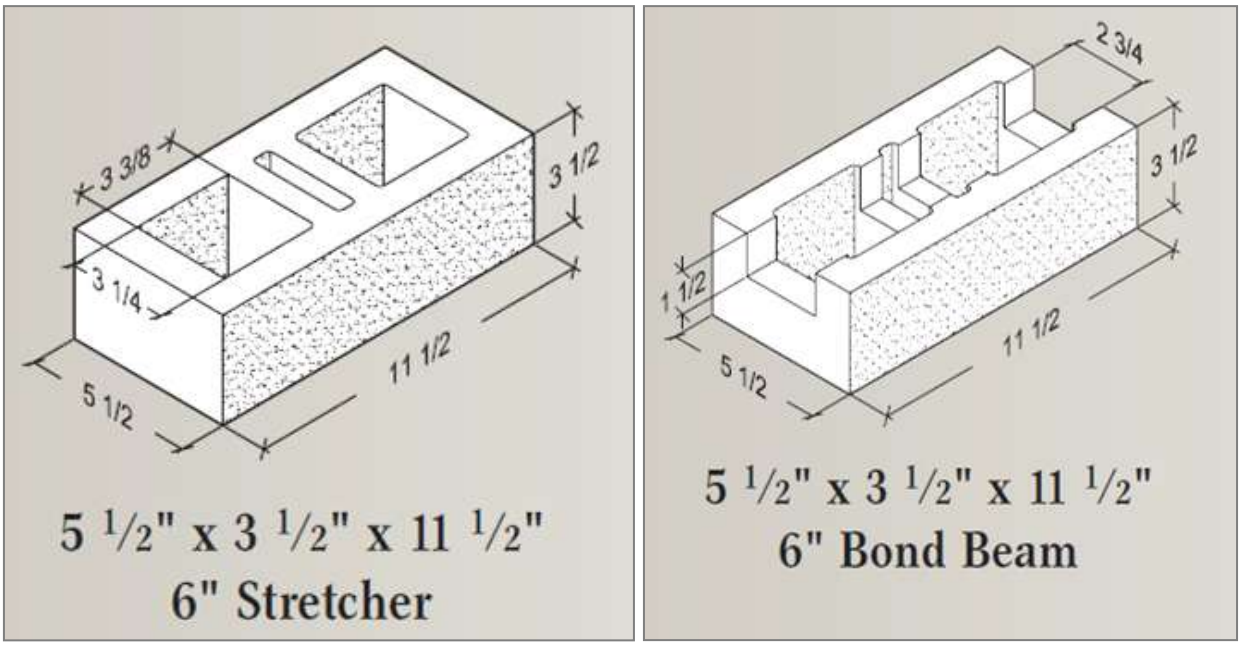

Figure 3.5: Clay Brick Dimensions (from Mutual Materials Catalog)

During construction, specimens were prepared to determine material properties. Three standard blocks were tested according to ASTM C140-11. Three mortar test cylinders with a 2-in. diameter and 4-in height were made with Type S mortar and were tested according to ASTM C780-11. Three grout prisms were constructed and tested according to ASTM C1019-11.The grout prisms were nominally 3.5-in. square by 7-in. high. Finally, three two-block prisms conforming to ASTM C1314-11 were constructed and tested. All material specimens were tested for compressive strength after completion of the panel tests at approximately 3 months after construction. The average compressive strength for each material is given in Table 3.2. Note that the compressive strength listed for the brick masonry units is based on an assumed net area of 50% of the gross area.

Table 3.2: Average Compressive Strength of Masonry Materials

	Masonry Units	Mortar	Grout	Masonry Prisms
Average Compressive Strength (psi)	11,530	3,270	6,940	4,920

Steel reinforcing bars used in the panels were standard Grade 60 with a measured yield strength of 64 ksi.

The two panels were constructed at the Composite Materials and Engineering Center at Washington State University. The construction took place in three phases. The first phase was to prepare the existing footing. It consisted of grinding the surface of the footing; drilling holes for the dowels, anchoring the dowels in the footing with epoxy, and spreading a thin layer of gypsum cement to smooth the surface of the footing in preparation for placing the neoprene pad and foam strips.

For the second phase, professional masons were hired to build and grout the test panels. The clay bricks were placed in running bond with face shell mortar bedding (3/8 in. mortar thickness). During this second phase, grouting of the panels took place as well as construction of the masonry and grout prisms.

The second phase is illustrated in Figures 3.6 and 3.7.

Figure 3.6: Construction Phase 2: Panel Construction

Figure 3.7: Construction Phase 2: Grouting

For the final construction phase, the loading beams were formed and poured. The forms were removed two days after grouting.

3.6 Test Setup

The footing of the specimen was anchored to a reaction floor with 1.25-in. diameter steel rods. Steel bracing was placed at each end of the footing to prevent sliding of the footing on the reaction floor during the test. Three identical hydraulic jacks with a 5-in. stroke and operated under a constant pressure applied axial (vertical) load onto the panel. The jacks had an individual rated capacity of 10,000 psi corresponding to maximum capacity of 120 kips of applied force per jack. The first panel was tested with a 20-kip axial load and the second with an initial axial load of 50 kips, which was later changed to 40 kips. The pressure to be applied was determined from Equation 3.1.

$$\boldsymbol{Pressure\ Gauge\ reading} = \frac{\boldsymbol{Specified\ Axial\ Load\ (kip)}}{\boldsymbol{360\ kip}} * \boldsymbol{10000psi} \qquad \text{Equation 3.1}$$

These jacks were connected in parallel thus maintaining equal pressure to each jack. The upward forces from the jacks were resisted by a box beam attached to a sliding trolley system. This arrangement enabled the jacks to move with the panel while maintaining a constant pressure and creating a “free” boundary condition at the top of the panel. Horizontal loads were applied to the panel by a 22-kip hydraulic actuator through the top loading beam. This actuator was controlled by a computer.

The panel was restrained from out-of-plane movement by a lateral bracing system.

The 22-kip capacity hydraulic actuator was attached to a steel frame on one side and to the loading beam on the other side. Drilled steel plates were placed on the ends of the concrete loading beam and were then tightened with four 1-in. diameter rods. The test setup is shown in Figure 3.8 and Figure 3.9 (North direction on the left).

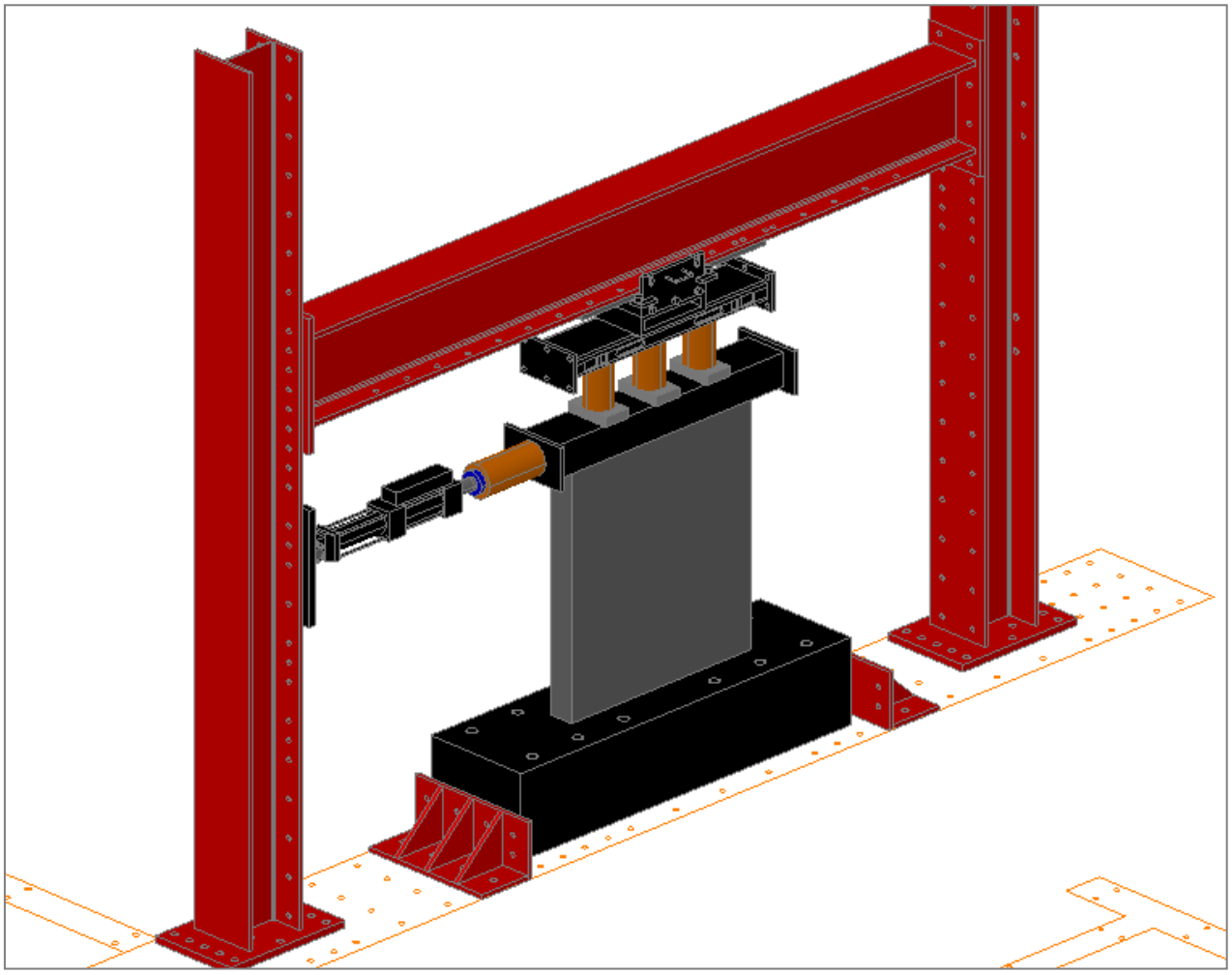

Figure 3.8: 3D View of Test Setup

Figure 3.9: Test Setup

3.7 Instrumentation

Four string potentiometers, one mechanical displacement gauge and a load cell attached to the horizontal actuator were used to monitor the response of the panels during testing.

One potentiometer (pot) (labeled as P4) with a 20-in. stroke was connected to the loading beam at the height of the load application and served to monitor the global lateral displacement of the panel during testing. The other end of this pot was connected to a rigid frame that was isolated from the main test frame. Two other pots (labeled as P2 and P3) with 10-in. strokes were placed at the North and South toes of the panel to measure the vertical displacements of the toes of the panels during testing. Finally, a fourth pot (labeled as P1) with a 2-in. stroke was placed at

the base of the panels to measure horizontal sliding of the panels. The mechanical displacement gauge was positioned against the footings to measure any movement of the footings on the laboratory floor. During testing, no significant sliding of the footings was observed (measured displacements were less than 0.001 in.). The positions of the potentiometers and the mechanical gauge are shown in Figure 3.10.

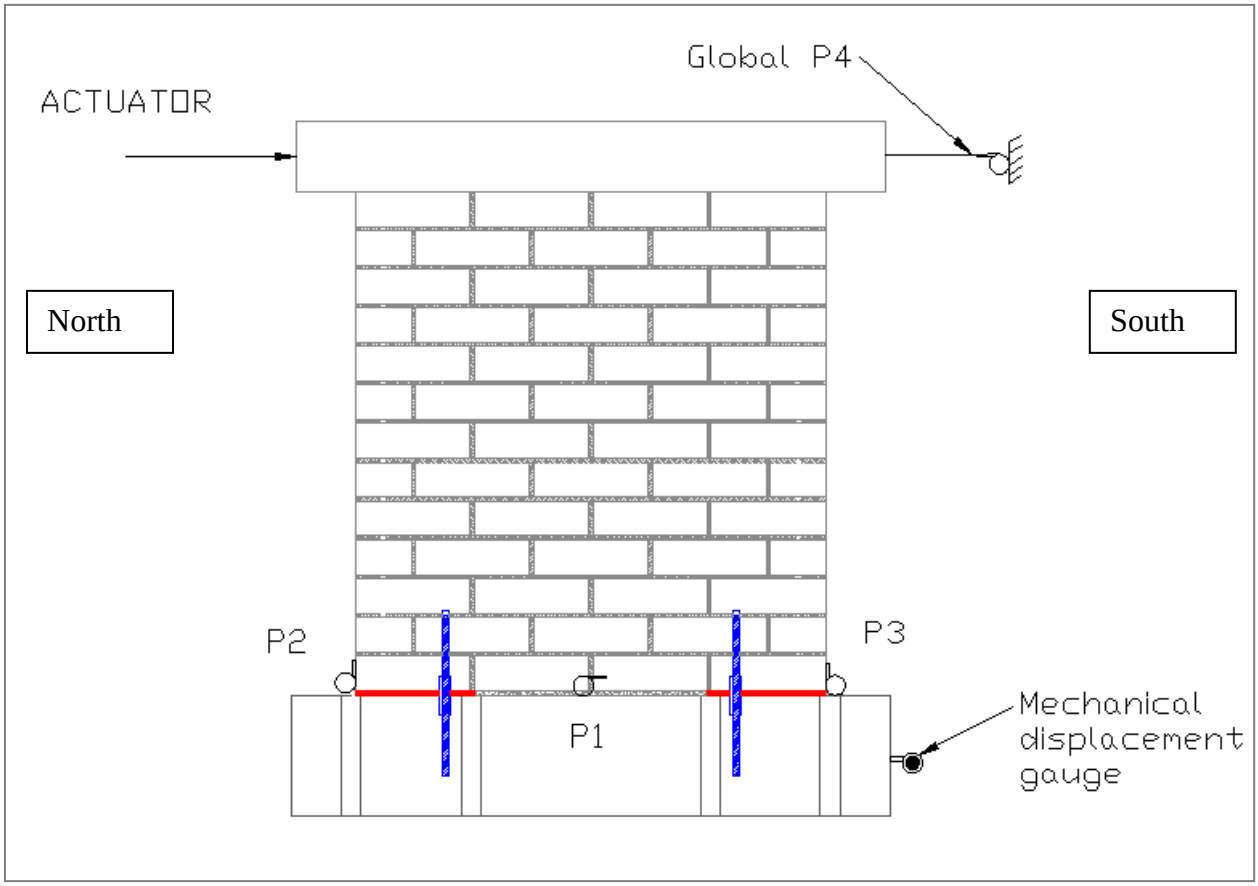

Figure 3.10: String Potentiometer and Gauge Locations

3.8 System Control and Data Acquisition

Two separate computer system were used for these tests. One computer controlled the 22-kip hydraulic actuator by sending information on the load, loading rate, and loading direction.

The second computer was used to collect and record data from the string potentiometers. A flow chart for the signals from the different computers and actuators is shown in Figure 3.11.

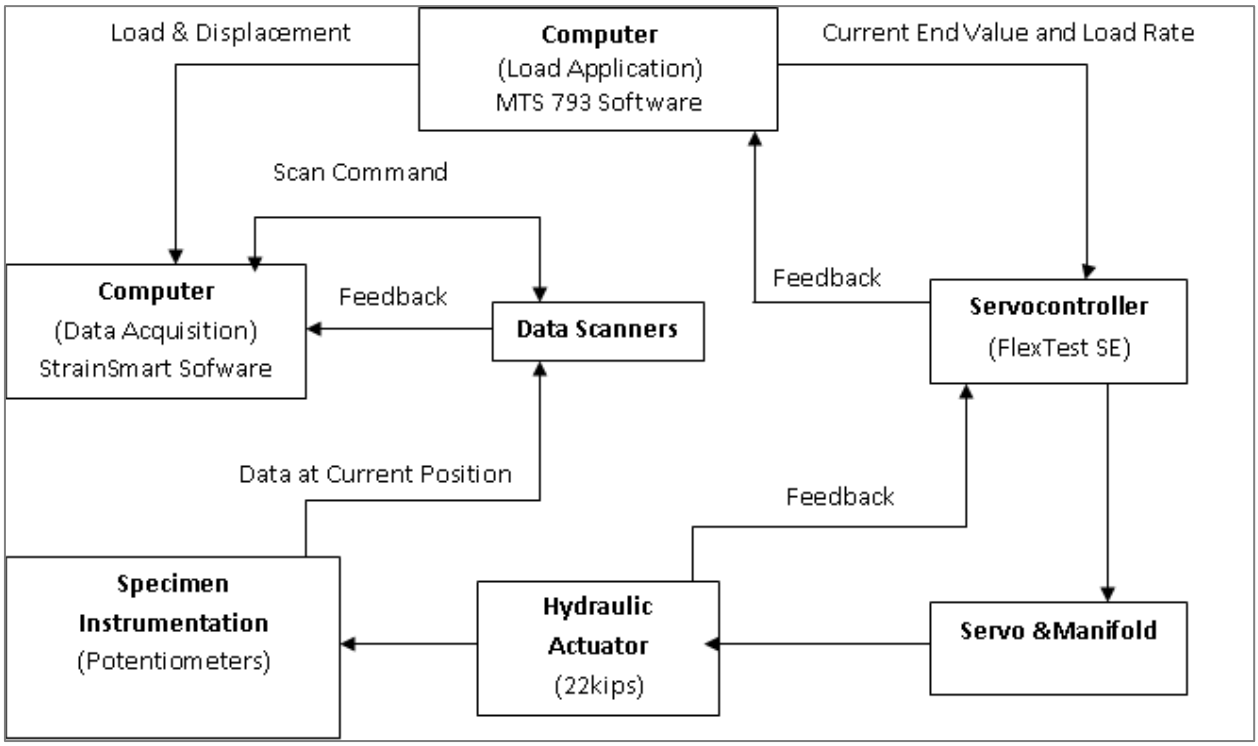

Figure 3.11: System Control Flow Chart (adapted from Sherman, 2011)

3.9 Test Procedures

The panels were subjected to slowly-applied, cyclic lateral loading using a prescribed pattern of input displacements. Axial load was maintained at a constant 20 kips during testing for Panel 1. For Panel 2, axial load was applied at a constant 50 kips for the first 3 cycles. Then, as the maximum capacity of the horizontal jack was reached during the third displacement cycle, the axial load was reduced to 40 kips for the remaining cycles.

The sequence of twelve horizontal displacement cycles is presented in Figure 3.12. Testing was stopped after completion of these twelve cycles. The global displacement in the figure corresponds to displacements of the top of the panel (measured by pot P4). The circle in the

figure represents an error in the intended loading pattern whereby Panel 1 was pushed to 2 in. instead of 1.5 in. As will be evident in the later discussion of results, this error did not significantly impact the behavior of the specimen.

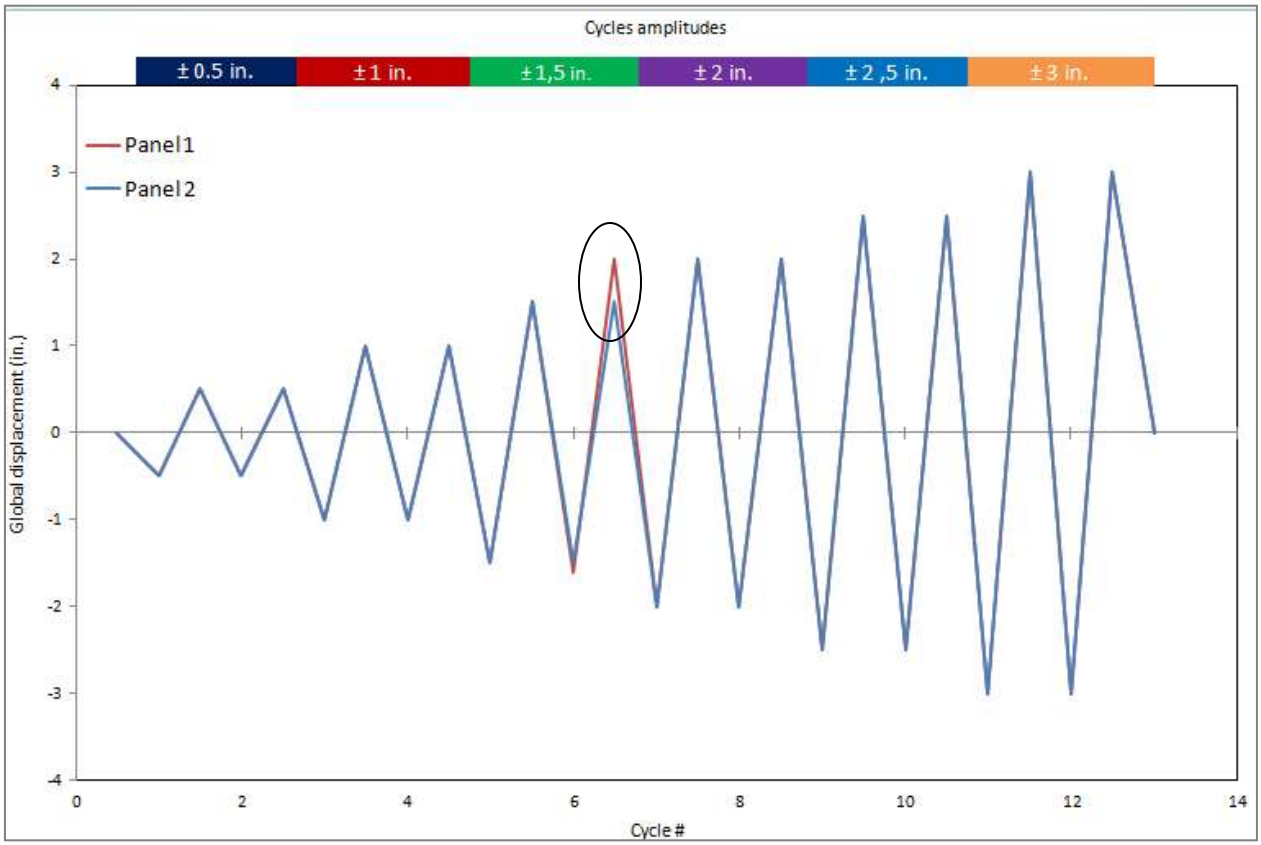

Figure 3.12: Loading Cycles

Testing of Panel 1 took place at the WSU Composite Material and Engineering Center on September 17, 2012. Panel 2 was tested on September 19. Both tests were completed in about 3.5 hours. Horizontal loads were applied at a rate of 0.5 in. /min. The tests commenced with pushing the panel to the South. Recording of the potentiometers data was started before the axial load application and stopped after the release of the same loads. This sequence allows for analysis of the influence of the axial load application and release on the panels.

CHAPTER 4: RESULTS OF PANEL TESTS

4.1 Introduction

Results for the two masonry panel specimens tested in this study are presented in this chapter. Results presented include test observations, load-displacement hysteresis curves, vertical displacements at the ends of the panel, and sliding displacements. Photos are presented that illustrate the observed behavior and damage to the panels during testing.

4.2 Panel 1

4.2.1 Test Observations

During testing, Panel 1 exhibited rocking behavior with little damage (see Figure 4.1 and Figure 4.2). At the end of testing, some cracks developed in the end of the panel and spalling of the faces of several bricks occurred on the West side as well as at the toes of the panel. Visual observations made during testing are listed in Table 4.1

.

Figure 4.1: Side View of Panel During Testing Showing Rocking Behavior

Figure 4.2: Rocking Behavior and Uplift of One End

Table 4.1: Visual Observations for Panel 1

Load (kips)	Disp. (in.)	Cycle	Test observation
1.49	0.38	1.5 in.	Onset of Crushing in North toe
1.06	0.5	2 in.	Onset of Crushing in South toe
4.85	0.305	2.5 in.	Sudden Spalling of a brick at base
-6.47	-2.68	3 in.	Minor Crushing South toe
10	2.4	3 in.	Spalling continues at base
5.4	2.8	3 in.	Minor Crushing North toe
-5.4	-0.1	3 in.	Splitting of brick in North toe - narrow face
0.5	0.687	3 in.	Splitting of brick in North toe – side

The uplift of the panel characterizing the rocking behavior is shown in Figure 4.3. Complete crushing of the foam is also shown in the figure; however, it can be seen that the foam remained intact.

Figure 4.3: Uplift of the North and South Ends of the Panel

4.2.2 Damage

Only minor damage occurred to the panel as a result of inputting the lateral displacements. Photos showing the observed damage are presented in Figure 4.4.

Figure 4.4: Damage to Panel 1

Photos of Panel 1 after completion of the test and removal of the panel from the footing are shown in Figure 4.5. No permanent damage was observed in the neoprene pad, but the steel dowels were bent at their base in a manner indicating shear yielding. The foam strips were compressed to a very thin sheet.

Figure 4.5: Photos showing Panel and Dowels at the End of the Test

4.2.3 Vertical Displacements Along the Length of the Panel

The vertical displacements measured by potentiometers P2 and P3 at the same time for peak displacements of pushing and pulling loading are provided in Figures 4.6 and 4.7. It can be seen in the figures that the center of rotation of the panel is located around 12 in. from the center of the panel (corresponding to 3/4 of the panel length). This location is approximately at the interface of the neoprene pad and foam strip. It is evident that, when the panel rocks, the compression force on the neoprene is concentrated near the end of the neoprene pad.

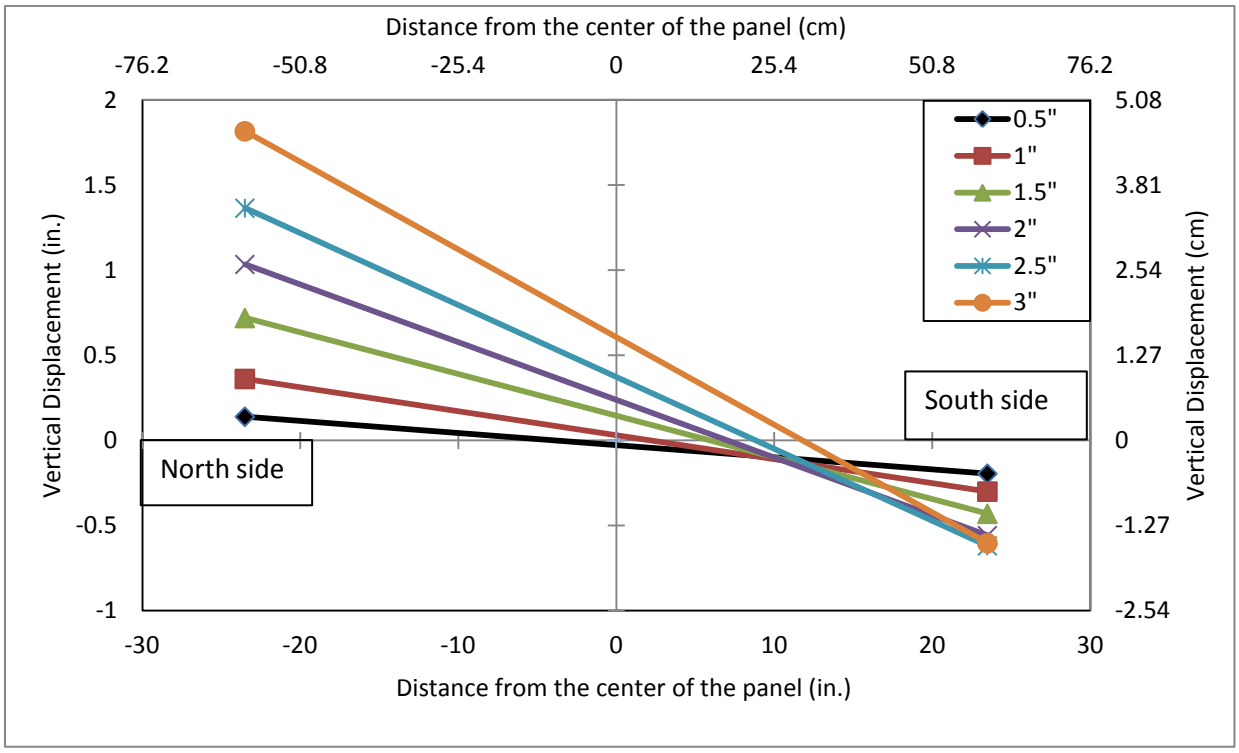

Figure 4.6: Measured Vertical Displacements for Pushing

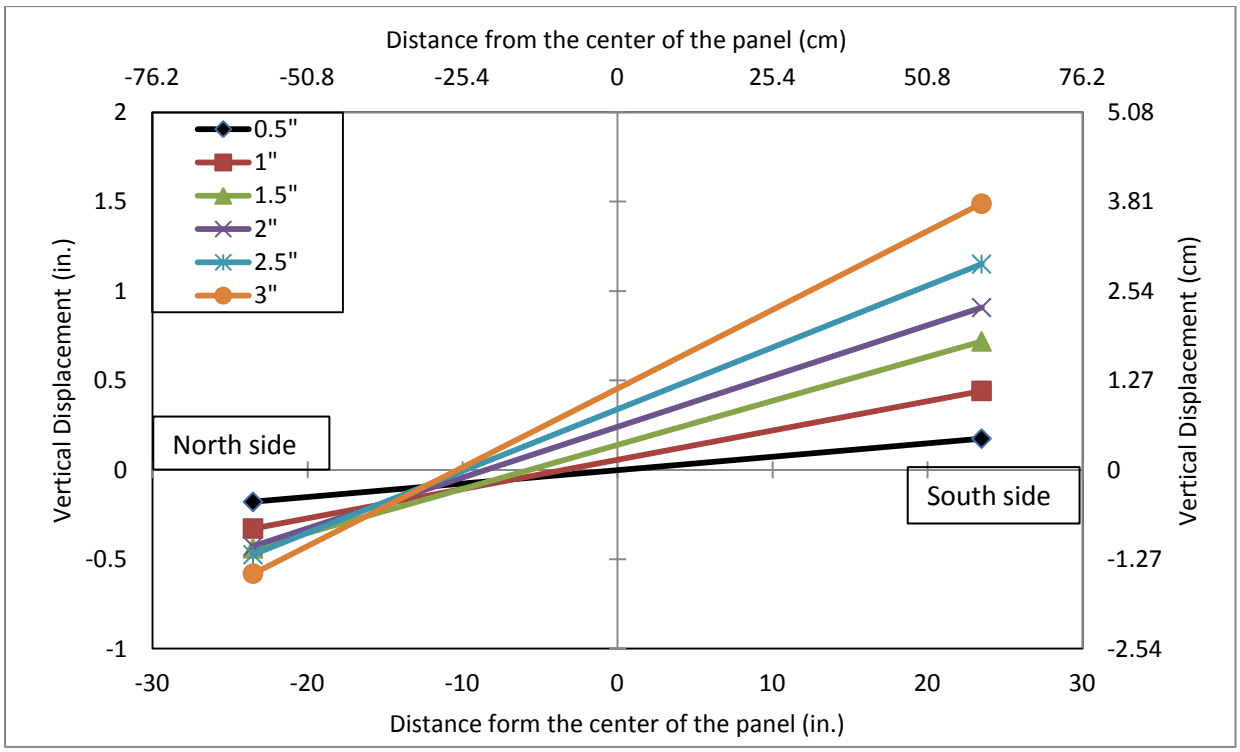

Figure 4.7: Measured Vertical Displacements for Pulling

4.2.4 Load-Displacement Curves

Hysteresis Curves

The load-displacement curves based on the global displacements of the panel (from Pot 4) are presented in Figure 4.8. The hysteresis curves are reasonably symmetric and show an approximately bilinear behavior, with a load plateau starting at around ± 0.5 in. (± 5 kips) and continuing until around ± 1.5 in. (± 6 kips). At displacements greater than 1.5 in., the specimen stiffens and the load increases above 6 kips to reach another load plateau around 13 kips. The areas under the curves are relatively small until stiffening of the panel begins.

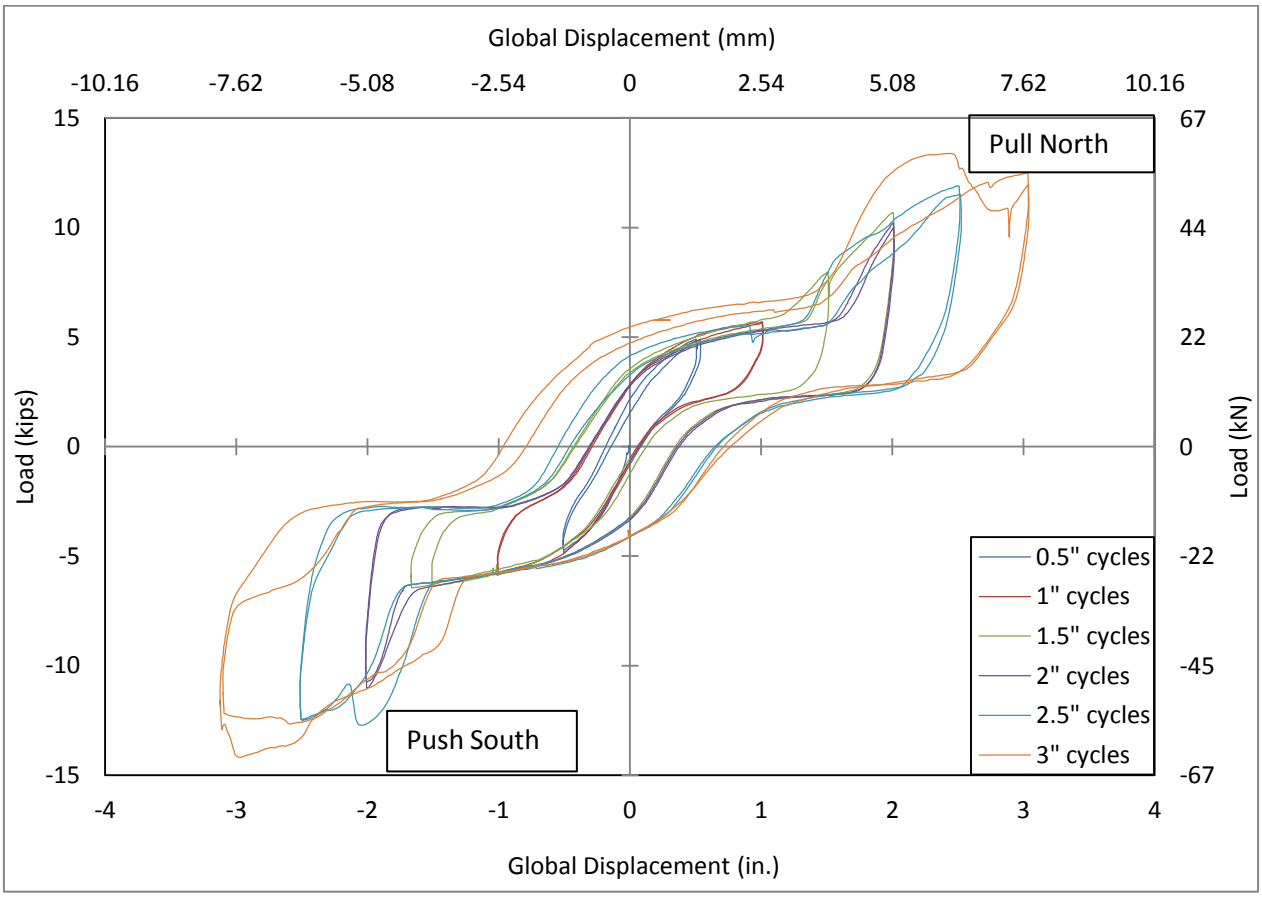

Figure 4.8: Hysteresis Curve for Panel 1

Panel Uplift

Plots of the vertical displacements at both ends of the panel are presented in Figure 4.9. The first plot is of the North Pot (P2), and the second plot is of the South Pot (P3). The two sets of curves are reasonably symmetric and reach a maximum negative displacement of around -0.5 in., corresponding to the crushing of the foam (which was originally 0.5-in. thick), and a maximum uplift of around 1.5 in. A plateau starts at around 0.2 in. uplift and a load of around 5 kips. These values correspond to the onset of visual rocking of the panel.

The initial compression displacement due to the engagement of the axial force (20 kips) was small with a value of 0.014 in.

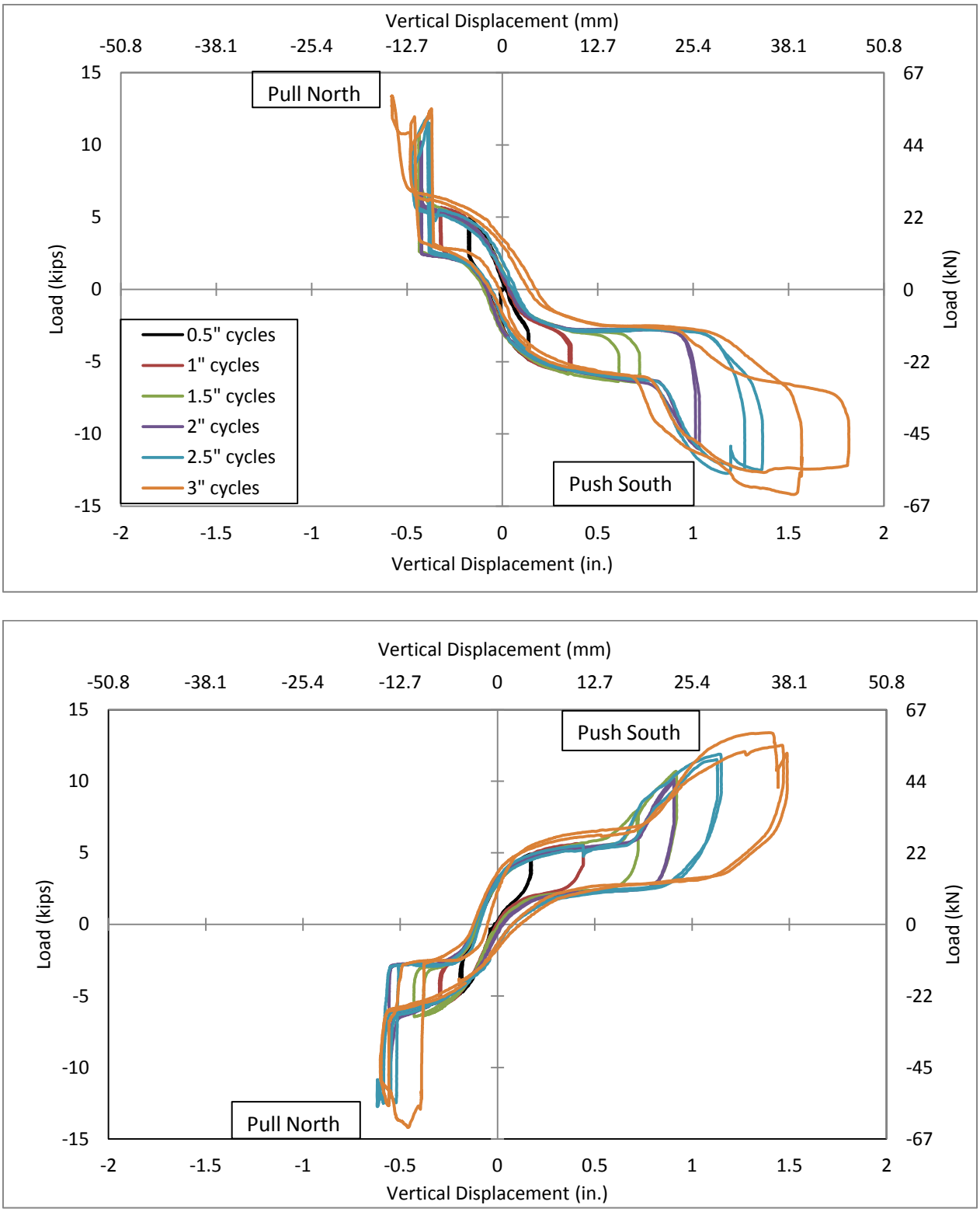

Figure 4.9: Uplifting and Crushing of P2 (top) and P3 (bottom)

Panel Sliding vs. Load

A plot of the measured horizontal displacements (sliding) of the panel vs. the applied horizontal loads is presented in Figure 4.10. The amount of sliding is small for low levels of applied lateral forces, but it becomes more significant as the applied load increases above 5 kips. The curves shown in Figure 4.10 are symmetric in both directions with a significant drop in applied load at the point of reversing the direction of loading. This drop in load is associated with friction between the neoprene pad and the panel as the load is reversed. A residual sliding displacement of about 0.5 in. was present at the end of testing. Note that, as mentioned before, the dowels were encircled with 0.25-in. thick insulation pipe foam, providing a gap between the grout and dowels. This gap needs to be compressed before engaging the dowels, which occurred during the 2.5 in. and 3 in. cycles. Also, when cycling to displacement levels of 2.5 in. and 3 in., an increase in load occurred just prior to 0.25 in. of displacement, followed by a load reduction. A possible explanation for this behavior is that, at larger displacements, the dowels had experienced plastic deformations introducing kinking and momentary locking of the dowels. The subsequent drop in load seen the curves occurs once the dowels begin to again slip vertically.

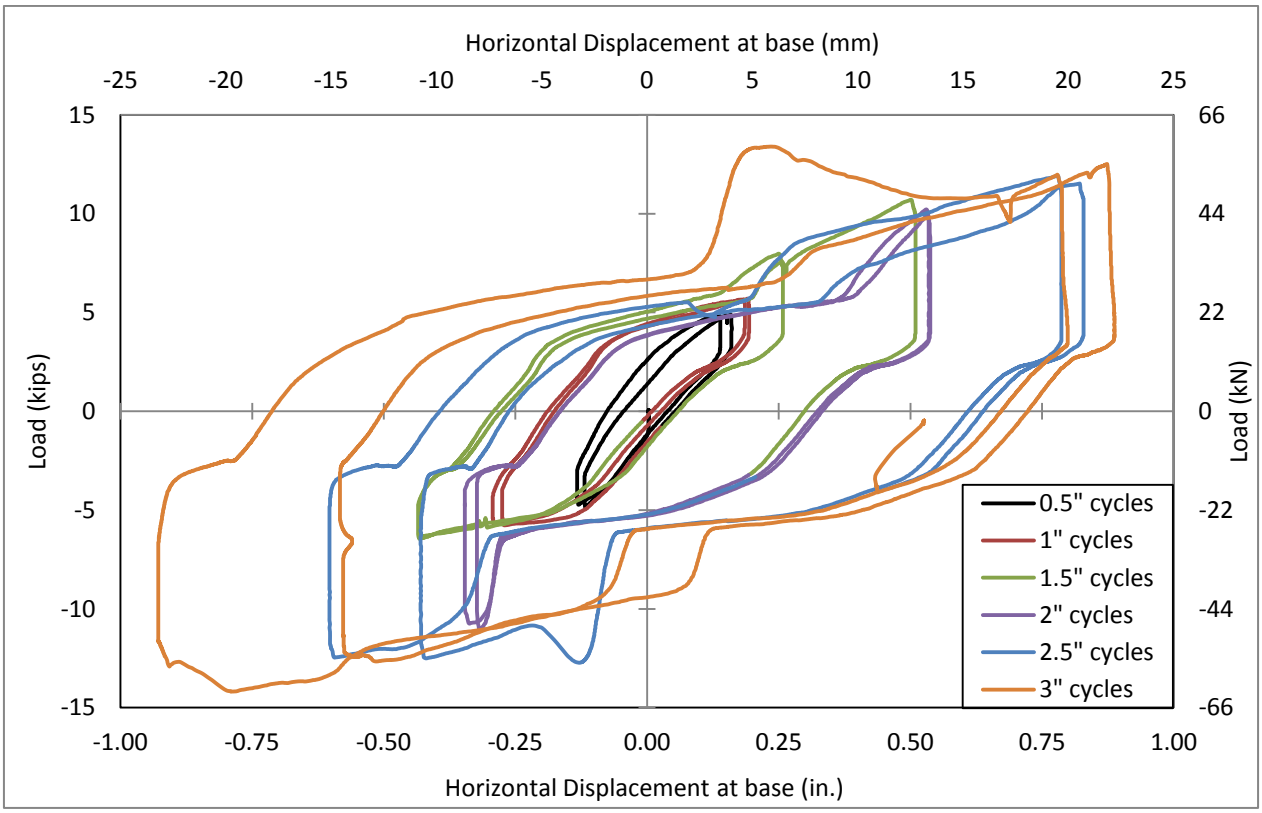

Figure 4.10: Sliding of Panel 1

Net Panel Displacement vs. Horizontal Load

A plot of the rocking load vs. net panel displacements defined as the global displacement minus the sliding displacement (P4-P1) is shown in Figure 4.11. The curves indicate a reasonably uniform rocking plateau of approximately 5 kips occurring between 0.25 in. and 1.25 in. of net displacements. Beyond 1.25 in. net displacement, the specimen stiffens and a second plateau is eventually reached at approximately 13 kips. Additionally, no perfect self-centering is observed. However, displacements at zero load are quite small (less than 0.25 in.).

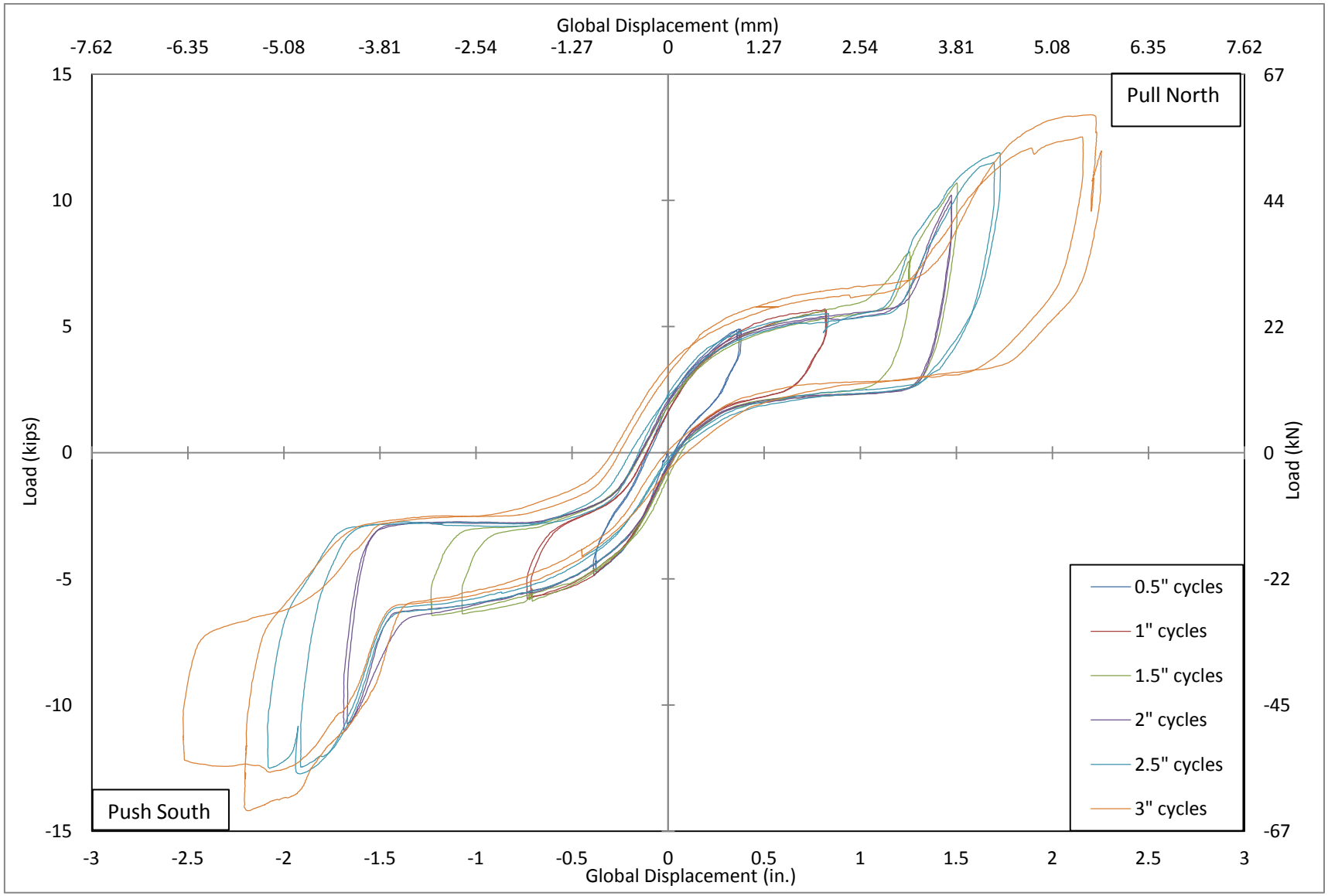

Figure 4.11: Load-Displacement Curve without Sliding

4.3 Panel 2

4.3.1 Test Observations

During testing, Panel 2 exhibited the expected rocking behavior for both the 40 and 50 kips axial loading. However, it experienced more substantial damage and a more complex response than was observed in Panel 1.

The rocking behavior of the panel at an advanced stage of the test is shown in Figure 4.12.

Figure 4.12: Rocking of Panel 2

The uplift and damage at the North toe is shown in Figure 4.13. It is clear that the toe is significantly uplifting. In addition, the behavior of the foam strips was different than for the first specimen. While both types of foam were fully compressed, the CCNS broke into pieces.

Figure 4.13: Uplift at North Toe

4.3.2 Damage

Observed damage includes spalling of the faces of bricks on both sides (East and West) of the panel at the base, numerous substantial cracks in the panel, and extensive toe crushing. Damage began early during the test. Visual observations made during testing are noted in Table 4.2. The damage was so extensive that the functionality of two potentiometers (P1 and P3) was lost during the test.

Table 4.2: Visual Observations for Panel 2

Load (kips)	Disp. (in.)	Cycle	Test observation
-10.5	-0.7	1 in.	Spalling East South brick
6.6	0.509	1 in.	Spalling West South brick
-9.7	-0.68	1 in.	Onset Spalling West Center brick
-1.3	0.21	1 in.	Spalling West Center brick + loss of P2
-3.3	-1.1	1.5 in.	Spalling East Center
0.2	-0.3	1.5 in.	Spalling West North : visible rebar
12.3	1.02	1.5 in.	Lateral Cracking East North
-12.5	-0.88	1.5 in.	Crack South Toe (8in. long vertically)
9.1	0.84	1.5 in.	Crack North Toe (3in. long vertically)
3.7	-0.1	1.5 in.	Onset of Toe Crushing at South
-4.4	0.14	1.5in. – 2in.	Change of Axial Load (50 kips ➔ 40 kips)
-10.1	-2.1	2 in.	Lateral Cracking East South
-15.3	-2.5	2.5 in.	Minor Toe Crushing at South
-10.9	-2.35	2.5 in.	Toe Crushing at South
18.1	2.4	3 in.	Advanced Toe Crushing at South + loss of P3

The spalling of the panel at both the East and West sides is shown in Figure 4.14.

Figure 4.14: Spalling on East (left) and West (right)

The crushing of the South toe is shown in Figure 4.15. Cracking first occurred in the brick units, followed by spalling of the bricks, and then crushing and spalling of the grout. Large residual vertical and sliding displacements were present in Panel 2 at the end of testing.

Figure 4.15: Toe Crushing at South Toe

The neoprene pad did not exhibit any damage at the end of testing. However, the foam strips were completely compressed. Additionally, the first two rows of bricks on both sides experienced widespread splitting and spalling, and extensive toe crushing occurred at both ends of the panel. Both dowels were severely bent. Photos after removing the panel from the footing showing the bottom view of the panel and the dowel bending are presented in Figure 4.16.

Figure 4.16: End-of-Test Photos

4.3.3 Vertical Displacements Along the Length of the Panel

The panel vertical displacements obtained from P2 and P3 at the maximum lateral displacements for each loading cycle are displayed in Figures 4.17 and 4.18. As was seen for Panel 1, the center of rotation occurred at the neoprene-foam interface or at around 12 in. from the geometric center of the panel. An exception to this was the first 2 cycles at small displacements where visual rocking had not started and the point of rotation was closer to the center of the panel (around 2 in. from the center). For the 3 in. cycles, the damage at the south toe caused the panel to rock on the toe, instead of on the neoprene pad. This shifted the center of rotation to around 16 in. from the center of the panel.

Results for the 3 in. curve are not displayed in Figure 4.18 because of the loss of P3 due to toe crushing. However, it seems that the center of rotation did not move during pulling. It stayed at around 12 in. from the center (3/4 of the wall length) because minimal damage was experienced at the North toe.

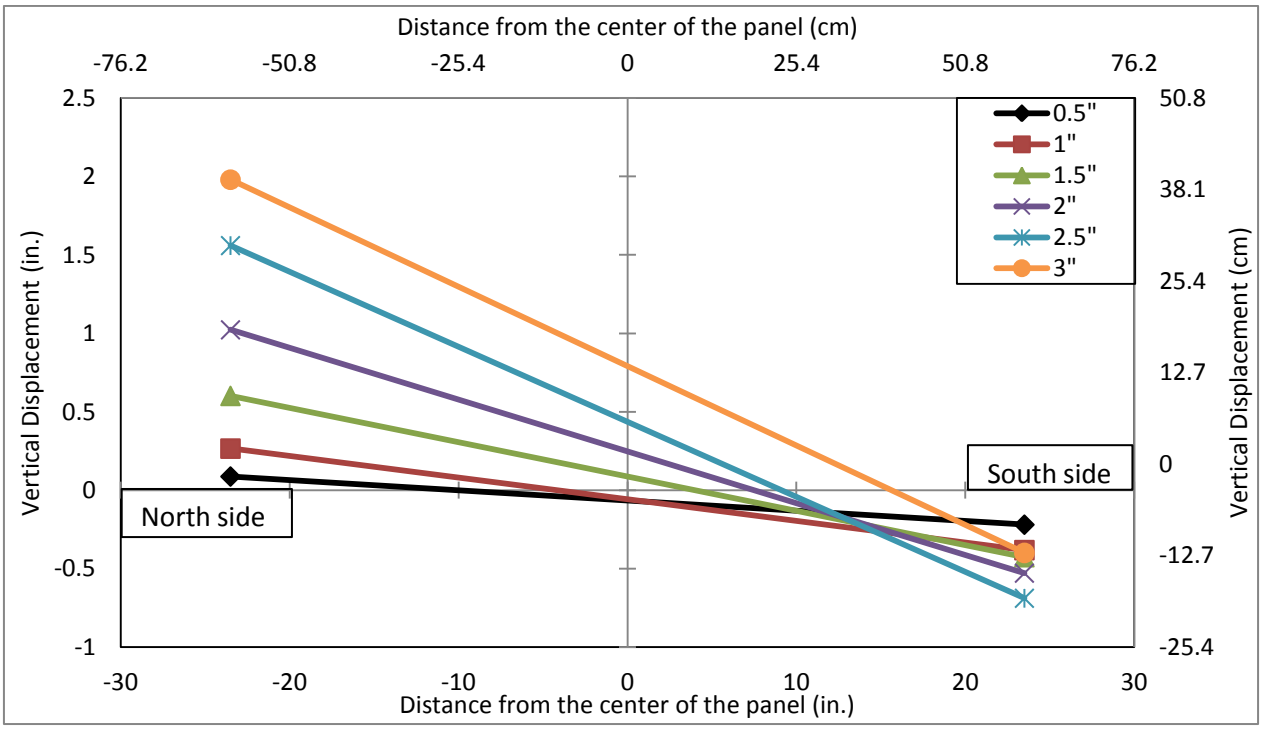

Figure 4.17: Measured Vertical Displacements for Pushing

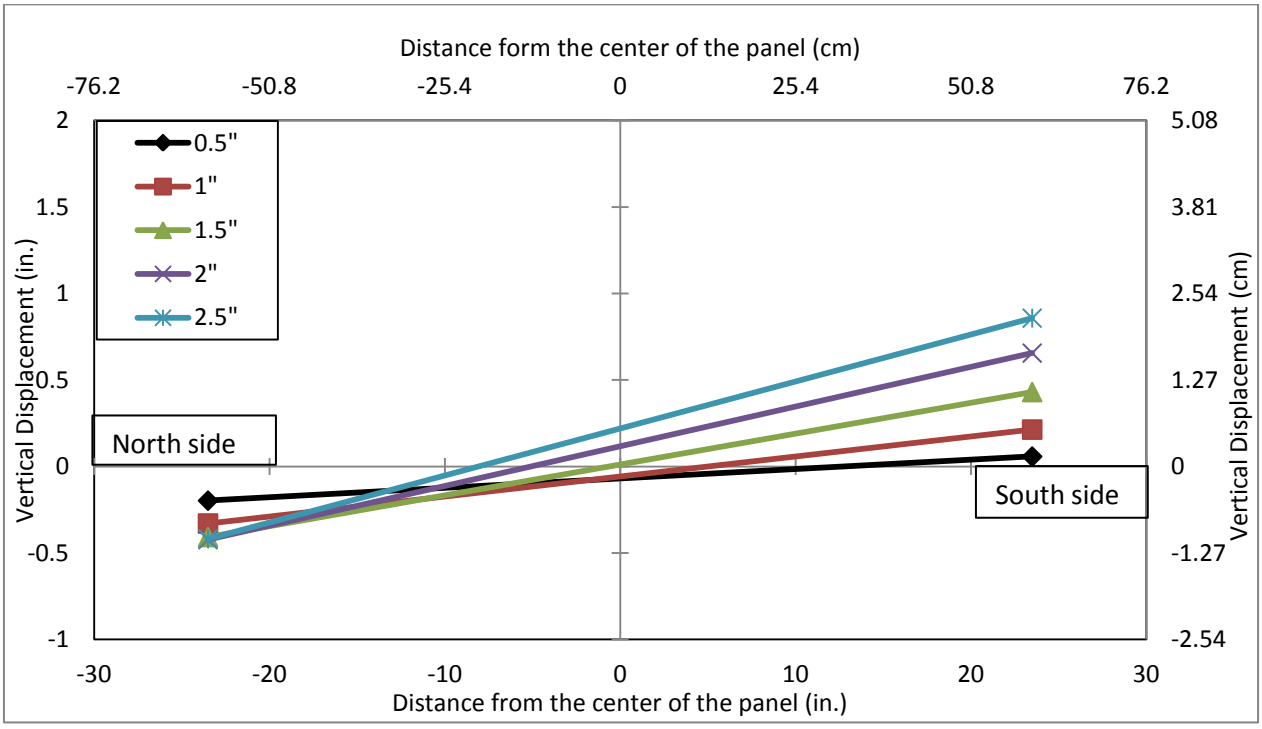

Figure 4.18: Measured Vertical Displacements for Pulling

4.3.4 Load-Displacement Curves

Hysteresis Curves

The load-displacement curves based on the panel global displacements (P4 potentiometer) are presented in Figure 4.19. The hysteresis curves are symmetric for the 0.5 in. and 1 in. cycles. Rocking seemed to begin during the 1 in. cycles. For the cycles beyond 1 in., the required load to push the specimen was somewhat higher than the load required to pull the specimen.

The effects of damage to the South toe are evident at two locations in the figure: on the left end of the curve with a decrease in stiffness, and at the abscissa intersection where the curve progressively shifts away from the origin.

When pulling (positive loads), a repeating curve can be seen with a plateau at a load of approximately 18 kips occurring between global displacements of 1.5 in. and 3 in.

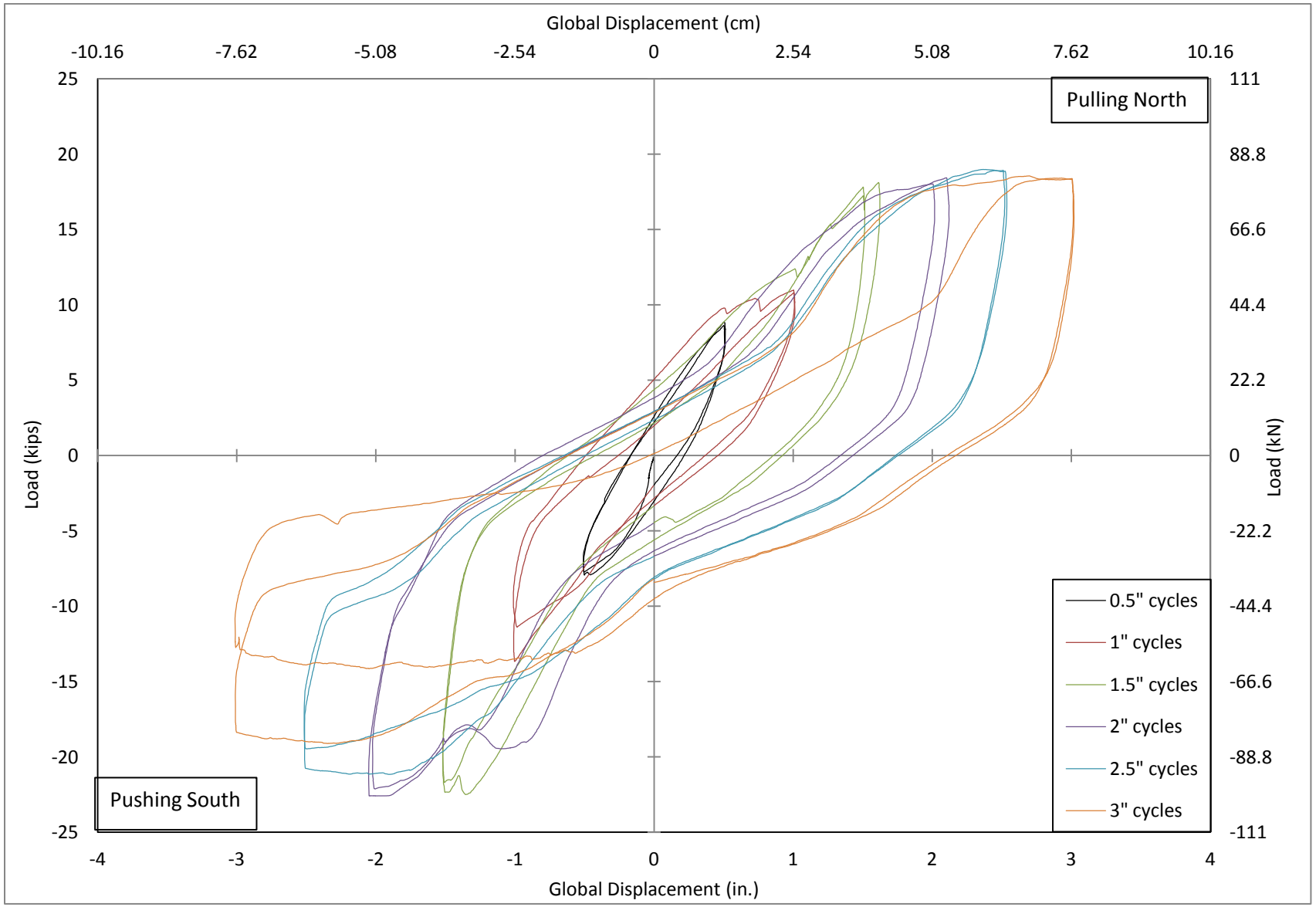

Figure 4.19: Load-Displacement Curve for Panel 2

Panel Uplift

The recorded vertical displacements at both toes are presented in Figure 4.20. The curves are symmetric until significant damage began during the 1.5 in. cycles.

The first curve represents displacements of the barely damaged North toe obtained from P2. The effects of a decrease in stiffness and the damage to the other toe are evident in the right side of the graph. A consistent compression of -0.5 in. at the North toe can be seen for most cycles except for the last 3 in. cycle. It is likely that this exception is due to the consequences of the toe crushing at the opposing toe. With this crushing, the entire structure begins to lean thus causing the displacement of -0.4 in. in compression. The maximum vertical uplift of 2.25 in. is associated with the crushing of the South toe. The initial displacement due to the application of the 50-kip axial load caused a 0.065 in. compression in the panel.

The second curve represents the South toe vertical displacements (P3). The initial compression due to 40-kip axial load is 0.07 in. Toe crushing can be seen when the maximum compression reaches -0.78 in. due to the crushing of the toe (the foam was nominally 0.5-in. thick). This created a shift in the rotation. The vertical uplift is then reduced to 0.85 in. maximum. Once again, a plateau at around 18 kips can be observed.

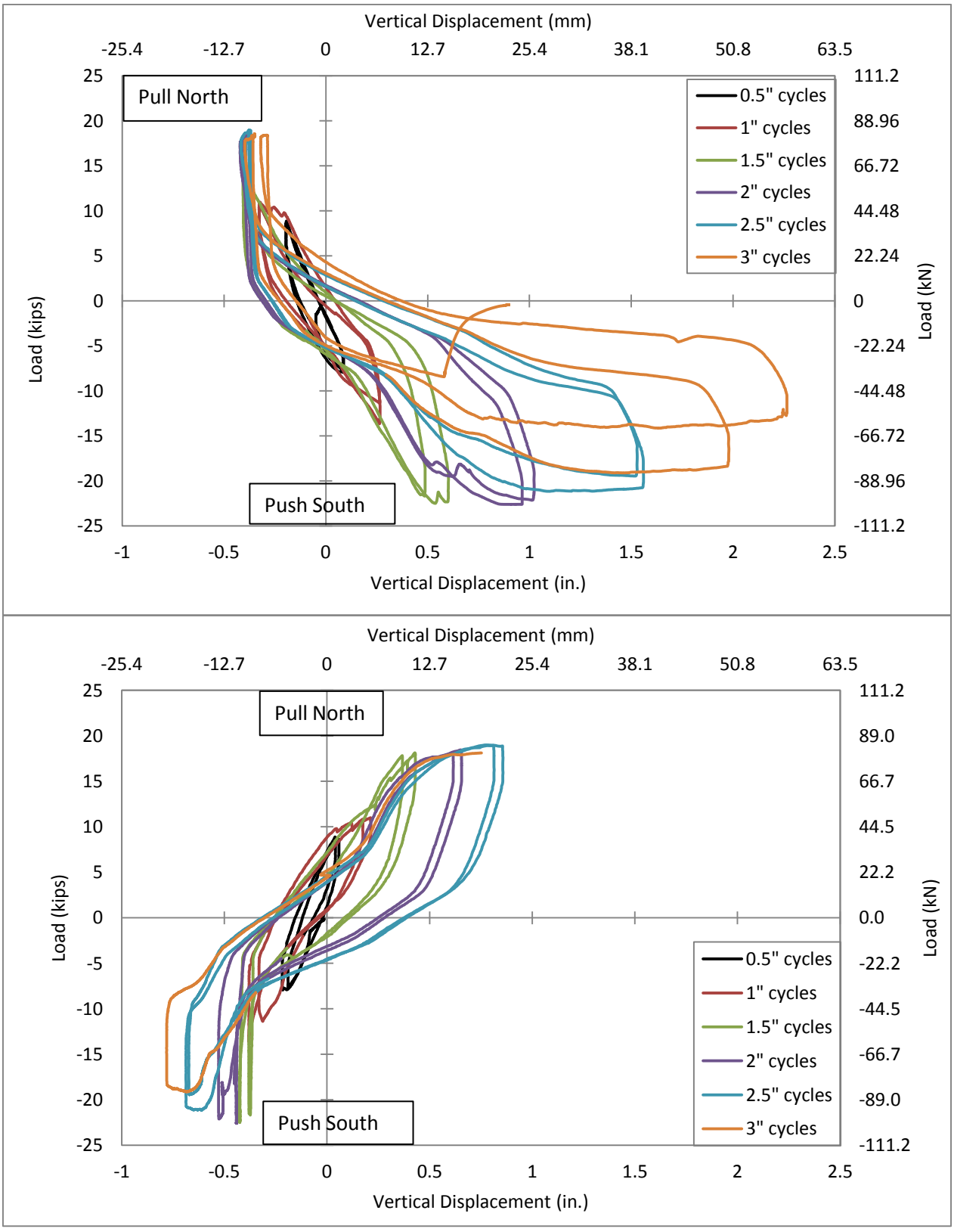

Figure 4.20: Load-Vertical Displacement Curves for P2 and P3

Panel Sliding vs. Load

The specimen experienced significant sliding displacements. However, the potentiometer P2 was lost during the 1 in. cycles due to spalling of the bricks. Consequently, no sliding measurements were obtained after the loss of the potentiometer.

The sliding displacements until the loss of the potentiometer are shown in Figure 4.21. Symmetrical curves are shown for the 0.5 in. displacement cycles. At the half cycle of 1 in. symmetry is lost. This can be seen with the 0.6 in. offset as opposed to the 0.4 in. symmetric offset. Due to damage and sliding, no self-centering is observed after this point.

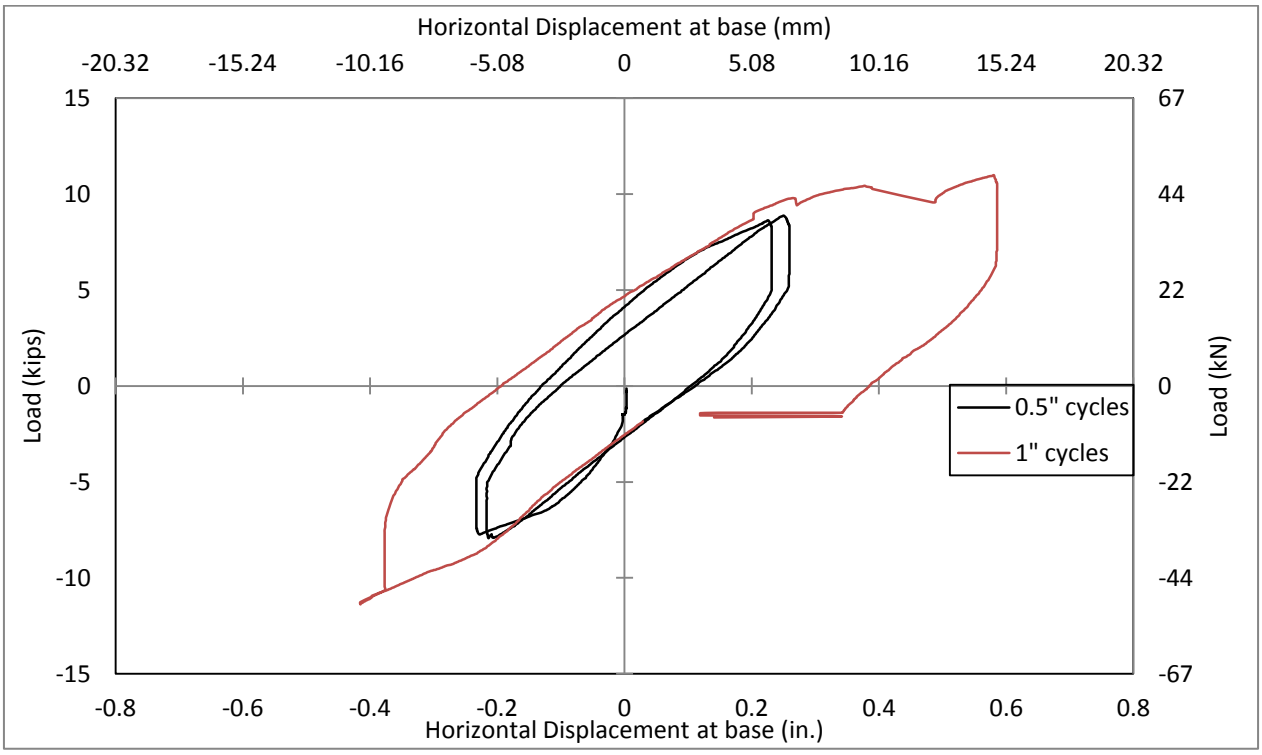

Figure 4.21: Sliding of Panel 2

Net Panel Displacement vs. Horizontal Load

As already mentioned, it was not possible to measure sliding displacements during the full duration of the test. Nevertheless, a comparison can be done before the loss of the potentiometer.

Both load-displacement curves based on the net panel displacement are presented in Figure 4.22. Similar to the results for Panel 1, a narrower curve is seen after removing the sliding displacement.

The net panel displacement (defined previously) corresponds to approximately half of the global displacement (recorded directly by P4):

- For the 0.5 in. cycles, peaks are at ± 0.26 in. when sliding is removed
- For the first 1 in. cycle, the extreme values are ±1 in. with sliding and ± 0.5 in. without sliding corresponding to the compression of the foam around the dowels.

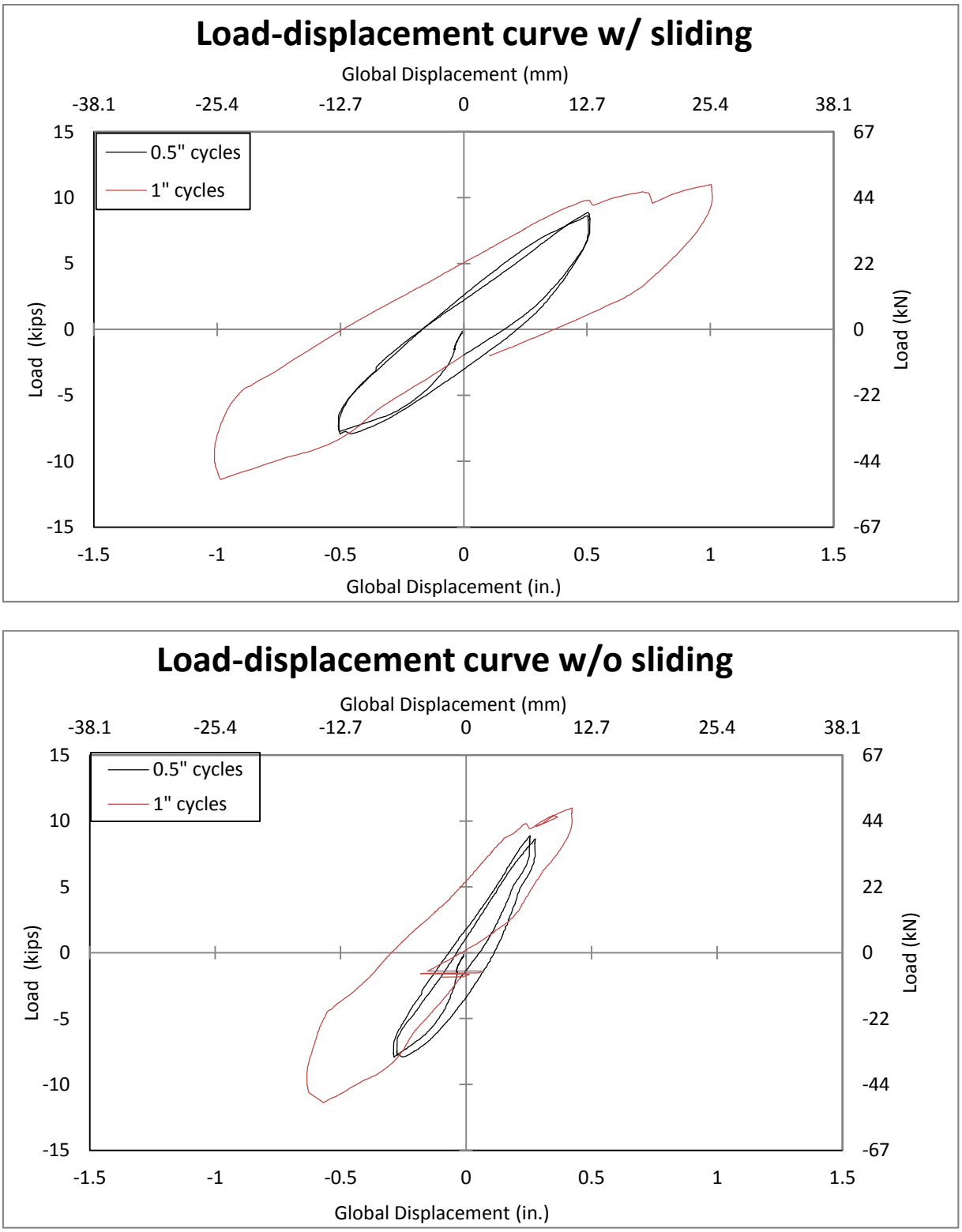

Figure 4.22: Comparison between the Load-Displacement Curves

4.4 Influence of the Axial Reduction from 50 kips to 40 kips for Panel 2

Due to reaching the maximum capacity of the 22-kip actuator during the 1.5 in. cycles for Panel 2, the applied axial load was reduced from 50 kips to 40 kips for the subsequent cycles. The influence of this change on the overall behavior and the damage is difficult to quantify. However, at the change, it resulted in a 400 lbs drop in lateral load as well as 0.035 in. movement upward in the panel. The uplift records for the 1.5 in. and 2 in. displacement cycles are shown in Figure 4.23. The circle in the figure shows where the change was recorded. It is evident that there was a change of stiffness between the two cycles, but this may also be due to the damage (see Table 4.2; the onset of a number of damage events happened during these cycles).

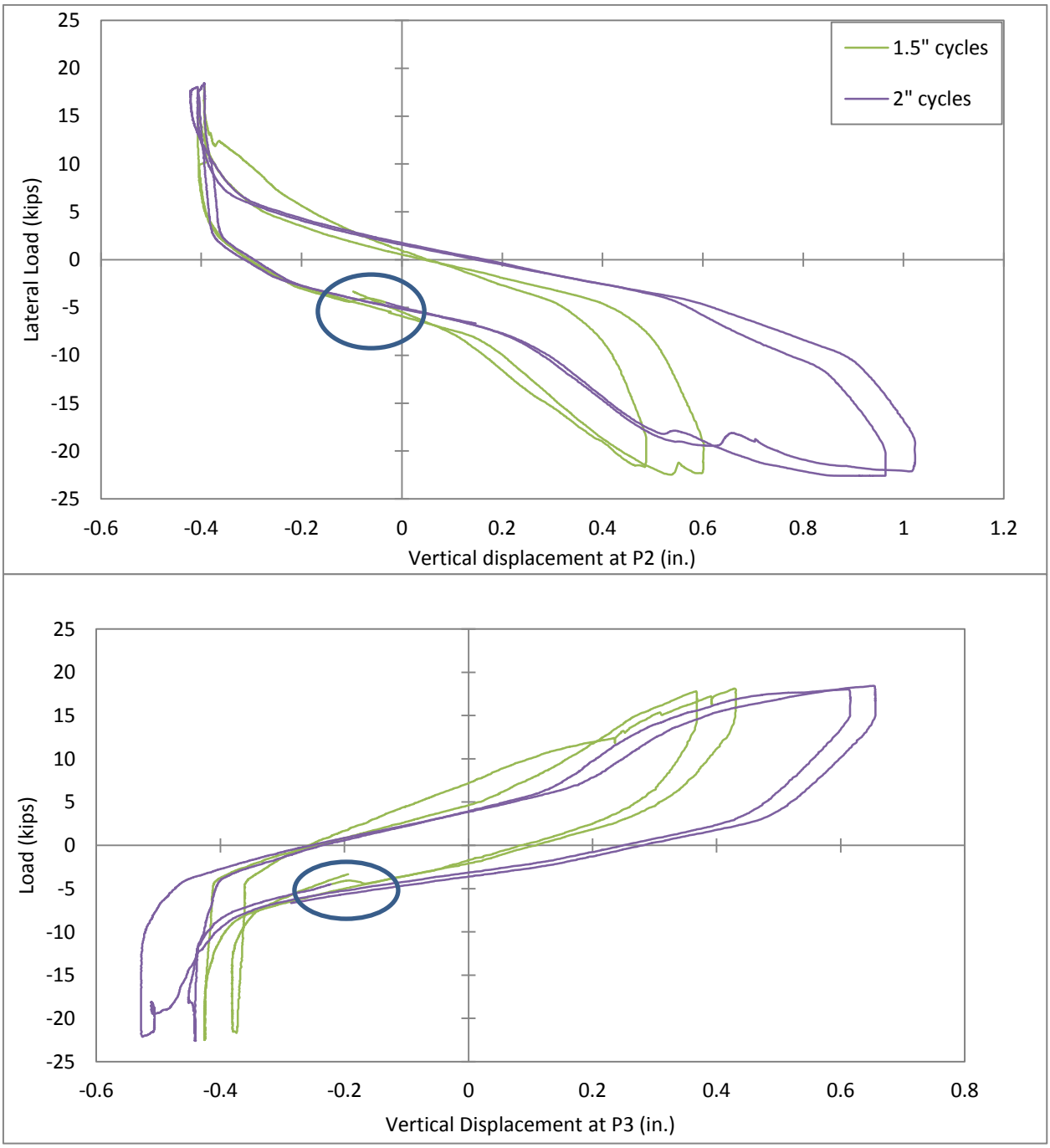

Figure 4.23: Influence of Axial Load Reduction

4.5 Influence of the Axial Load Change from 20 kips to 50/40 kips

Panel 1 was tested under 20 kips of axial load, while Panel 2 was tested with 50 kips (later reduced to 40 kips) axial load. Two major differences were observed from the tests of 2 panels.

This first difference is that Panel 2 experienced much more damage. The second difference is the amount of force that was necessary to cause rocking in the panel. Indeed, this is the reason for the change of axial load during the test of Panel 2. Consequently, Panel 2 had a higher stiffness than Panel 1 as shown on Figure 4.24.

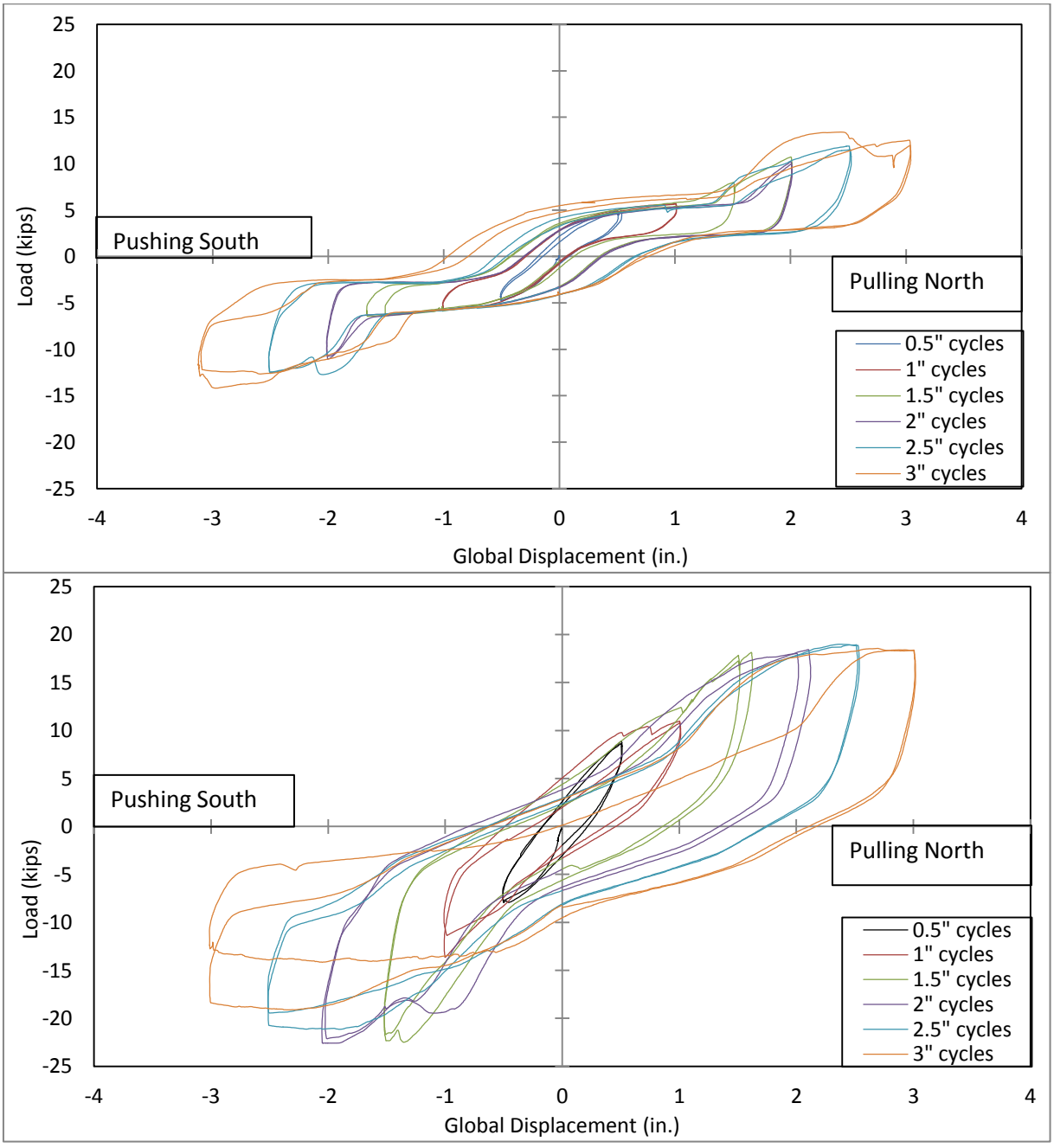

Figure 4.24: Load-Displacement Curves for Both Panels Depicting the Change of Stiffness

4.6 Summary and Conclusions from the Panel Tests

This chapter presented results from quasi-static cyclic tests performed on two rocking masonry veneer panels. Results presented include visual observations, load-displacement hysteresis curves and an analysis of the rotation observed in both panels. The effects of the higher axial loads used for testing Panel 2 are also discussed. Photos of each specimen during and at the end of testing were provided.

Panel 1 exhibited clear rocking behavior during testing. Very little damage, consisting of several spalled bricks and minor cracking in the panel, was observed in this specimen. After removal of the panel from the footing, bending of the dowels was evident as well as the complete compression of the foam strips. The neoprene pad exhibited no damage. At small lateral displacements, the center of rotation of the panel during testing was located close to the center of the panel. At this time, the panel had not started rocking and was oscillating on the neoprene pad. Rocking initiated at 0.5 in. of lateral displacement and the center of rotation shifted to the interface of the neoprene pad and foam strip, approximately 12 in. from the center of the panel. Two load plateaus were evident in the load-displacement hysteresis curves: the first plateau was at around 5 kips of in-plane load covering 0.5 in. to 1.5 in. of lateral displacements and was associated with rocking, and the second plateau was at around 13 kips and occurred towards the end of testing. Panel 1 experienced significant sliding on the footing, with nearly 1 in. of permanent displacement at the end of testing.

Panel 2 also exhibited rocking behavior during testing, but substantial damage occurred to the panel due to the larger axial loads. Splitting and spalling of the bricks above the neoprene pad on both sides of the panel and significant toe crushing at the South occurred during testing. After removal of the panel from the footing, complete compression of the foam strips was observed

similar to that for Panel 1, but the bending of the dowels was more significant. The centers of rotation for Panel 2 were located at the same places as Panel 1: close to the center of the panel for small displacements, and at 12 in. from the center once rocking initiated. The hysteresis curves were substantially different than those for Panel 1. They were not symmetrical, no clear plateau can be determined for rocking, and there was a plateau for positive load at around 18 kips near the end of testing. Significant sliding representing half of the input global displacements were recorded before the loss of the instrument measuring sliding. The larger axial loads for Panel 2 also resulted in increased lateral capacity and stiffness.

The special isolation details generally performed as intended in both panels. The detail enabled stable rocking in Panel 1 to drifts of around 2%, and no significant damage occurred even when displaced to drift exceeding 5%. The foam strips were completely compressed effectively creating voids at both ends of the panels. Sliding of the panels on the neoprene pads and shear yielding of the dowels dissipated energy during testing.

CHAPTER 5: ANALYSES, DISCUSSION AND COMPARISONS OF PANEL PERFORMANCE

5.1 Introduction

This chapter provides discussion of analyses performed to understand the behavior observed in the testing of the two panel specimens. Comparisons are made of the calculated loads to rock the panel with test results. The performance and effectiveness of the isolation details to produce rocking response and dissipate energy are evaluated. Differences and similarities of the two specimens are also discussed.

5.2 Rocking Load

Based on equilibrium principles and Figure 5.1, the load required to cause a unit value (1 in.) of uplift of the panel can be calculated as follows:

The assumptions are:

- Rotation on the interface of the neoprene-foam at 12 in. from the center of the panel based on the discussion in Sections 4.2.3 and 4.3.3;
- A weight (W) of 1450 lbs for the panel and loading beam, based on a assumed density of approximately 145 lbs/cubic foot for both components;
- The influence of the foam is neglected (treated as a void);
- The system is in static equilibrium and the sum of moments at the point of rotation is 0; and

- Second-order effects due to changes in geometry are not considered. It is recognized that these second-order effect would slightly increase the predicted rocking loads, particularly for larger lateral displacements.

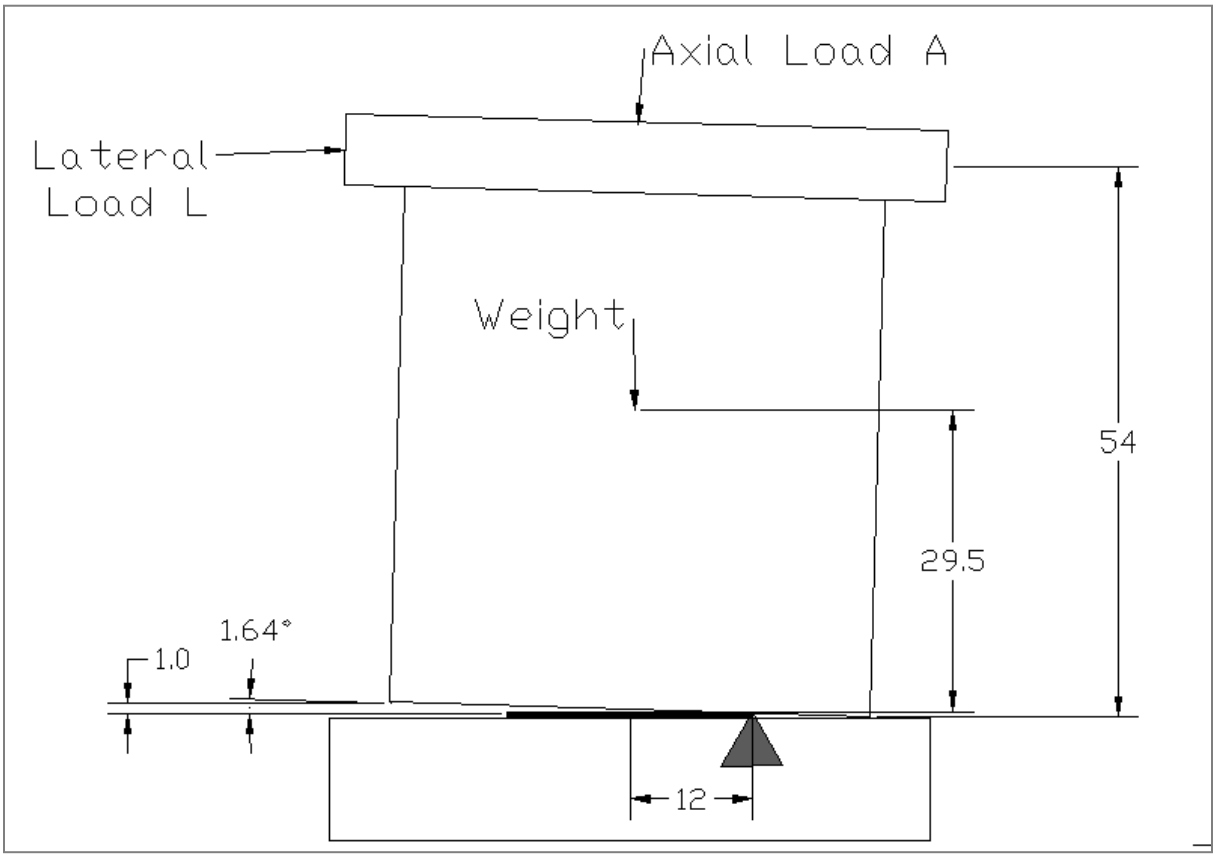

Figure 5.1: Static Calculation (dimensions in inches)

$$L = \frac{12*A+11.96*W}{54}\ in\ kips$$ Equation 5.1

The rocking loads determined from Equation 5.1 for the three values of axial load used in the tests for the panel specimens are listed in Table 5.1. The rocking load listed in the table for

Panel 1 compares well with the observed plateau at about 5 kips of lateral load corresponding to the onset rocking in this panel (see Figure 4.8 and 4.9).

Table 5.1: Required Lateral Load for used Axial Loads

A (kips)	L Required (kips)
20	4.77
40	9.21
50	11.43

For Panel 2, two axial loads were used:

- For A = 50 kips, the first two cycles do not reach the 11.43 kip lateral load required to activate the rocking mechanism. However, after exceeding this load on the third cycle (1.5in), the panel starts to rock as can be seen in Figure 5.2. The dowels get engaged as soon as the rocking mechanism is activated. This causes a greater stiffness which can be seen in Figure 5.3.
- For A = 40 kips, the dowels also get engaged as soon as the rotation starts, at a lateral load of around ± 9.2 kips. This behavior is evident in Figure 5.3.

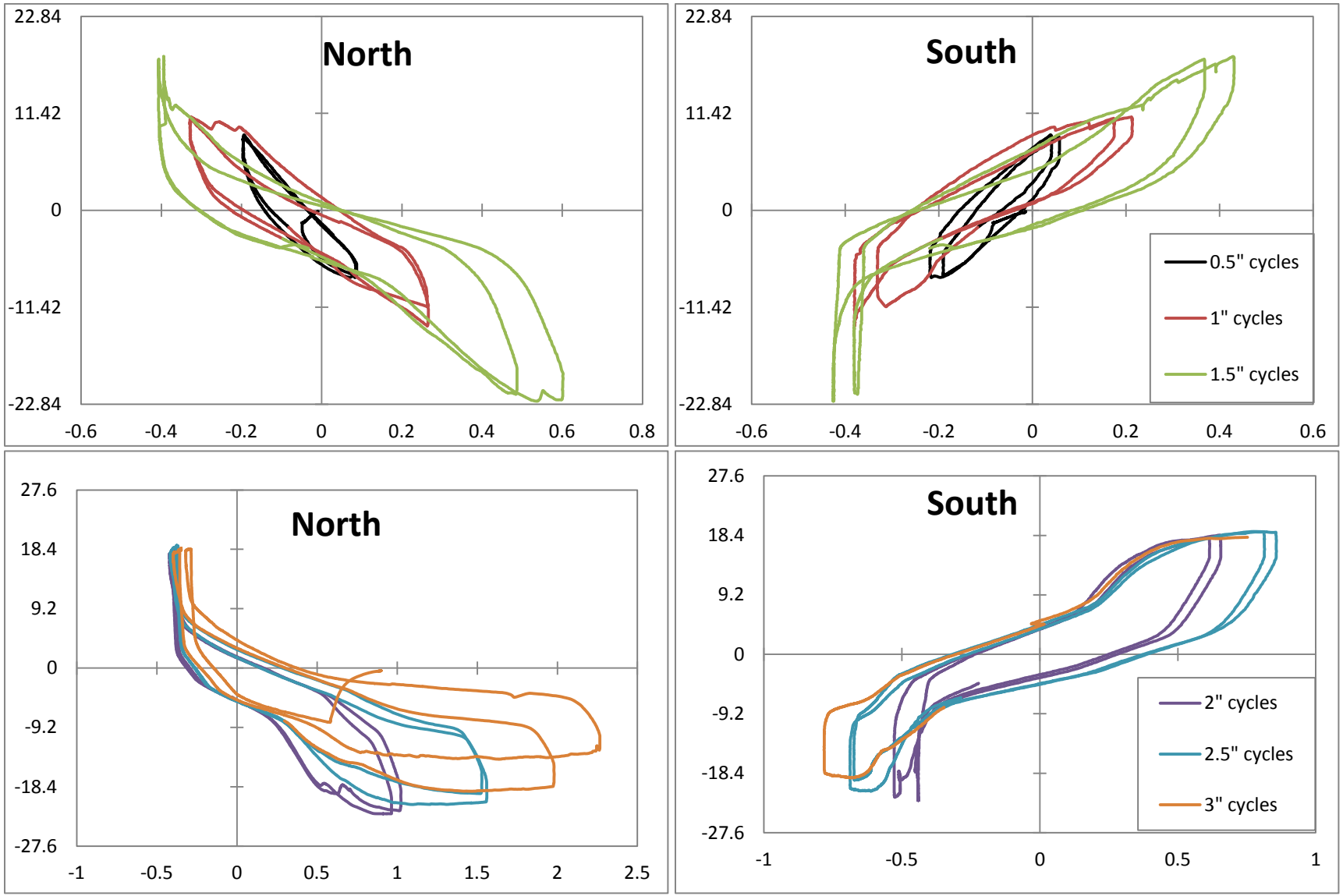

Figure 5.2: P2 and P3 Records for Panel 2.

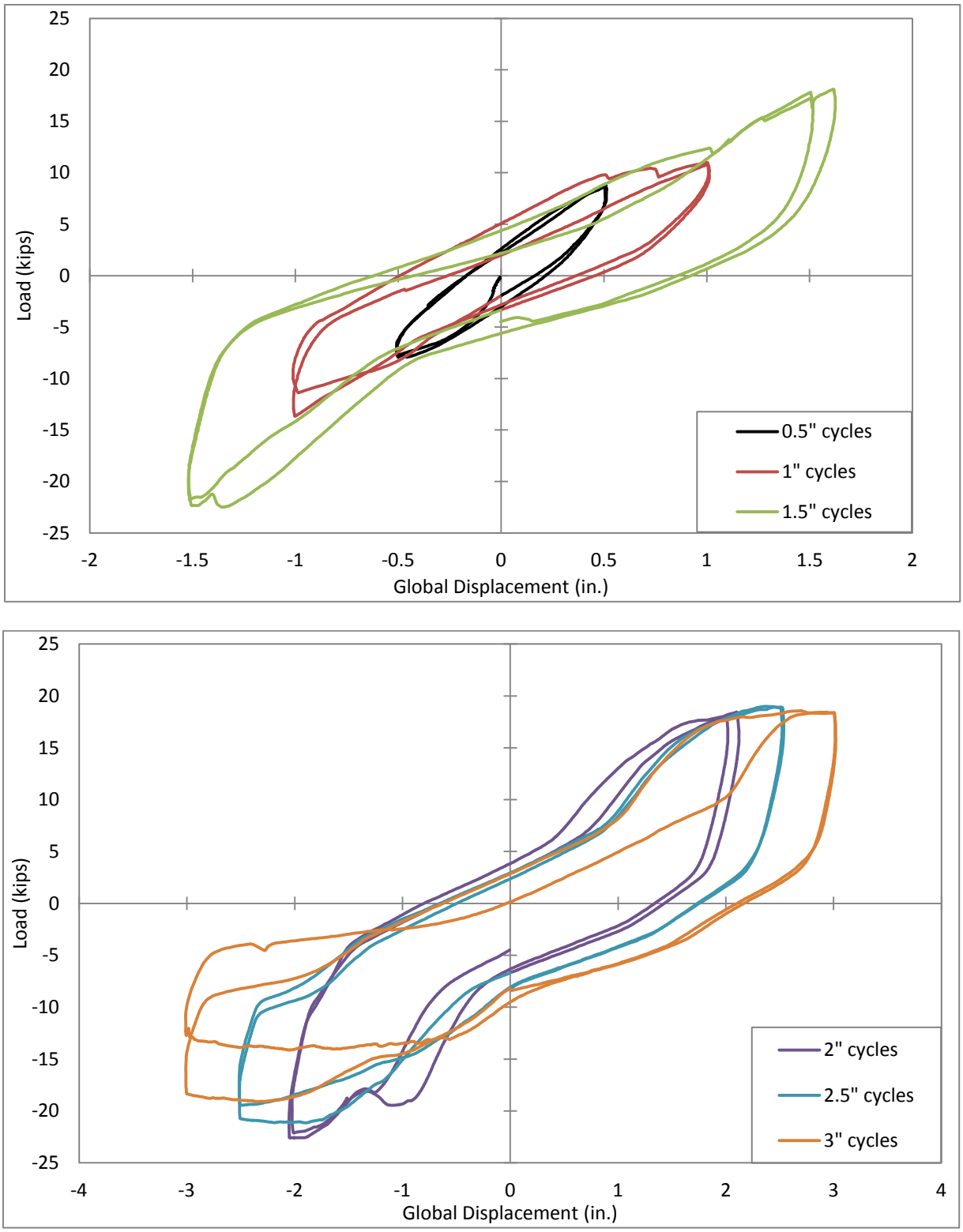

Figure 5.3: Load-Displacement Curves with 50 kip Axial (top) and 40 kips (bottom)

5.3 Dowel Yielding

Along with friction on the neoprene pad, the two steel dowels contributed to restraining the panel from sliding. At small displacements, the foam sleeve around the base of the dowels results in no loading of the dowels. As displacements increase, the sleeve compresses and the dowels are loaded in single shear. Eventually at large displacements, the dowels yield in shear and are severely deformed resulting in second-order effects. This mechanism is less predictable since the dowels are kinking and momentarily locking against vertical slip.

For Panel 1, a gain in load capacity at around 1.25 in. of lateral displacement is shown in Figure 4.11 and is likely associated with the dowels being engaged in shear. The dowels are encircled by 0.25 in. of foam. At panel sliding displacements greater than 0.25 in., the foam is compressed and the dowels engage and resist sliding, thereby increasing the lateral load capacity of the panel. A second plateau was reached during testing at a load of around 13 kips. The second plateau corresponds to the yielding of the dowels. The Masonry Design Standard provides Equation 3.9 (MSJC, 2011) which gives the shear strength of headed and bent-bar anchors as follows:

$$B_{vns} = 0.6 A_b f_y \qquad \text{Equation 5.2}$$

B_{vns} is the nominal shear strength of an anchor when governed by steel yielding (lb) and A_b the cross-sectional area of the anchor (in^2). Based on a yielding strength of 36 ksi for the A36 steel dowels, this gives a load of 13.3 kips to cause yielding of the two 5/8-in. diameter dowels. This level of shear load corresponds very closely to the plateau recorded in the test of Panel 1.

For Panel 2, the dowels seem to engage as soon as the rotation starts, at around 1 in. of global displacement (corresponding to 0.25 in. of uplift).

5.4 Behavior of the Neoprene Pad and Foam Strips

The compressive strengths of both types of foam strips are insignificant. However, the polystyrene foam strips remained intact after compression while the CCNS foam strips lost their integrity during testing, which makes the polystyrene foam the recommended material for this application.

As a result of the weak resistance in compression, the foam strips were completely compressed at the end of the test. Consequently, the neoprene pad is the only point of transfer of axial load to the footing. It also determines the center of rotation for rocking of the panels. With the panel resting on the neoprene, it changes the expected location of the center of rotation of a rigid block (at the toes) to an inner location (at the neoprene-foam interface). The presence of the foam strips has the effect of protecting the toes for small rocking displacements (less than approximately 0.5 in. in uplift that results in compressing the 0.5 in. thick foam).

Based on a Poisson's ratio of 0.5 for the neoprene, substantial lateral expansion would be expected from the axial loading, particularly once rocking starts and area of neoprene carrying axial loading is reduced. Such expansion was observed during testing, as can be seen in Figure 5.4, at the free edges of the panels. This lateral expansion of the neoprene is restrained by friction between the neoprene and the overlaying bricks and footing. Eventually, the outward friction force on the brick results in a brittle tension failure and spalling of the brick face due to tension forces. This spalling occurred in Panel 1 during the 2.5 in. cycles and in Panel 2 during the 1 in. cycles.

The boundary conditions on the neoprene are provided by only the panel and the footing. Therefore, the pad is free to move laterally and side-ways with only friction to impede it. With an

increase in lateral load, friction caused some large deformations in the neoprene, as shown on Figures 5.5 and 5.6.

Figure 5.4: Lateral Expansion of Neoprene

Figure 5.5: Neoprene Deformation in Panel 1

Figure 5.6: Neoprene Friction Reaction in Panel 2

5.5 Energy Dissipation

The total energy dissipated by the two panel specimens was determined based on the area inside the loop of the load-displacement hysteresis curves using the Trapezoidal Rule shown in Equation 5.3. The basis of this calculation is illustrated in Figure 5.7. It assumes a straight line between two consecutive points and calculates the area enclosed by the hysteresis loops.

$$E = \frac{1}{2}\,(\Delta_2 - \Delta_1)(L_2 + L_1) \qquad \text{Equation 5.3}$$

E refers to the energy between data points (kip-in.), Δ_1 and Δ_2 are the displacements (in.) and L_1 & L_2 are the load at the data points (kips).

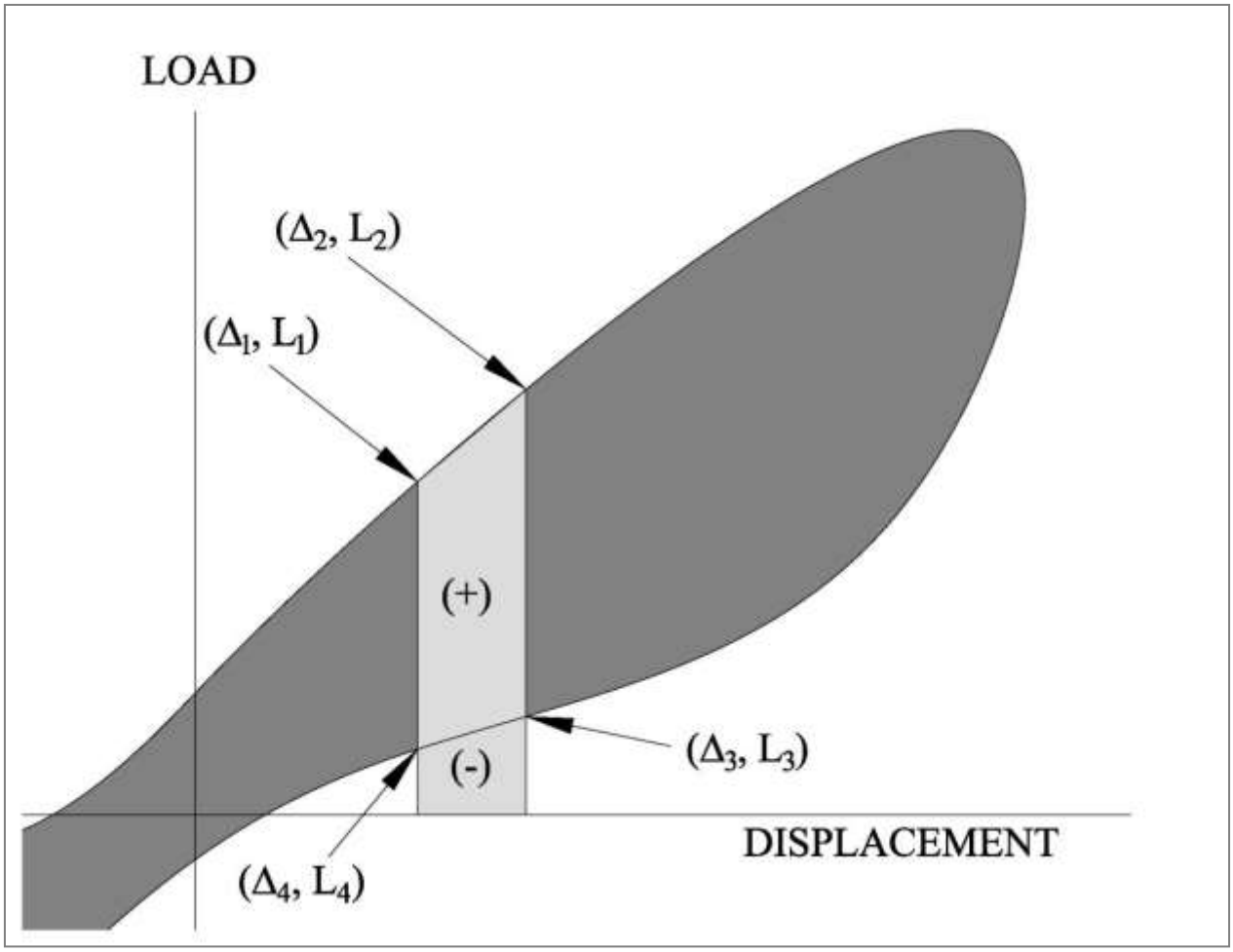

Figure 5.7: Illustration of Total Energy Equation (adapted from Snook, 2005)

Energy dissipation in the panels may be caused by the following five different potential mechanisms:

- Compression the foam, but it is clear that not much energy is required to achieve this process;
- Inelastic deformations in the panel, but the panel acted for the most part as a rigid body;
- Friction and sliding of the panels on the neoprene and deformation of this material (elastic and/or plastic);

- Bending and shear deformation of the dowels; and
- Damage to the masonry panel.

The relative contributions to energy dissipation are not the same for two specimens as they did not undergo the same amount of axial loading.

- Specimen 1 dissipated 214 kips-in., mostly through sliding of panel on the neoprene and plastic deformation of the dowels.
- Specimen 2 dissipated 467 kips-in. Since the axial and lateral loads were larger in this panel, it would be expected that more energy would be dissipated. Nevertheless, the energy dissipated before the onset of damage was is 97 kips-in. With the amount of damage experienced by this panel, it is hard to quantify the amount of energy dissipated by each mechanism. However, it is clear that more energy is dissipated through damage in Panel 2.

Cumulative energy dissipation is given in Figure 5.8 for both panels. The vertical colored lines represent the global lateral displacement at the engagement of the dowels (around 1 in. for Panel 2 and 1.25 in. for Panel 1). It can be seen that the energy dissipation increases significantly once the dowels get engaged.

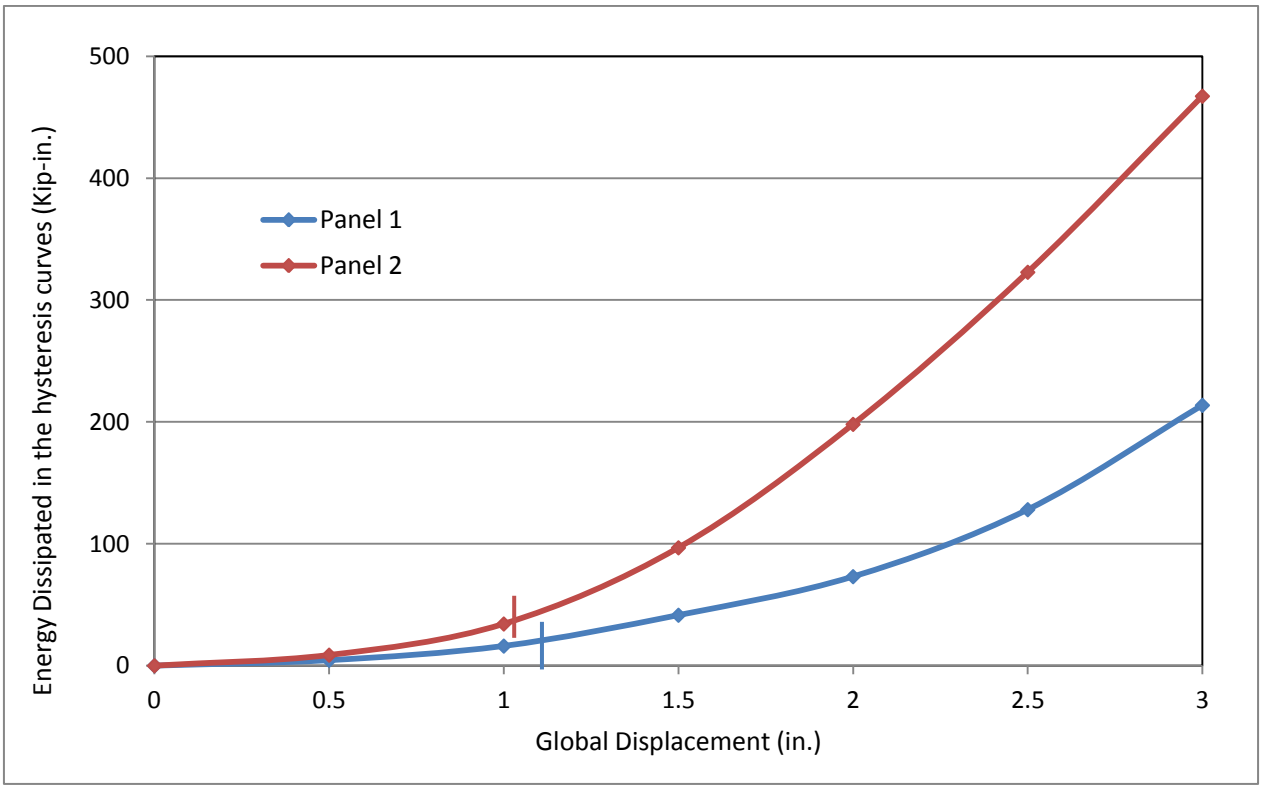

Figure 5.8: Cumulative Energy Dissipation for both Panels

In order to be able to compare the dissipation of energy between both panels, the calculated energy was divided by the axial load used for testing each panel and is presented in Figure 5.9. It can be seen the axial load is a main parameter in the energy dissipation capacity. For small displacements (less than 1.5 in.), both panels dissipated the same amount of energy per axial load. At larger displacements, the energy dissipation is greater in Panel 2, most likely as a result of the greater damage in this specimen.

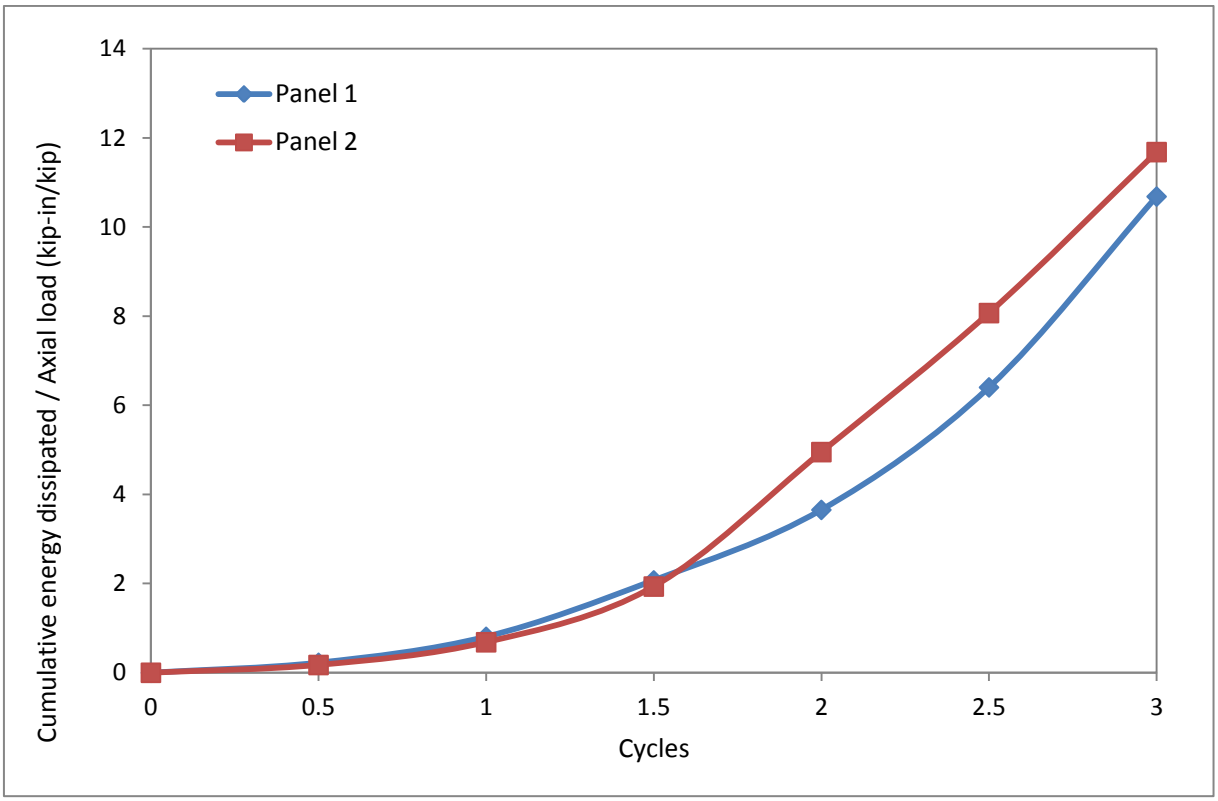

Figure 5.9: Normalized Cumulative Energy Dissipation for both Panels

Plastic deformation of the dowels resulted in significant energy dissipation. This is particularly obvious in Figure 4.11 which depicts the energy from only rocking. Once the dowels get engaged, creating a stiffer curve, the area under the curves is greater than the area before engagement. The neoprene behaved elastically, and the energy dissipated by the neoprene itself is small. However, the energy dissipated by friction and sliding at the neoprene interfaces is clearly significant. Figure 5.10 shows an idealized representation of load-displacement cycle for a body restrained by friction. By comparing this figure with Figure 4.10, a similar behavior can be observed. It can be concluded that the energy dissipated from friction and sliding at the interface is significant, particularly at larger lateral displacements.

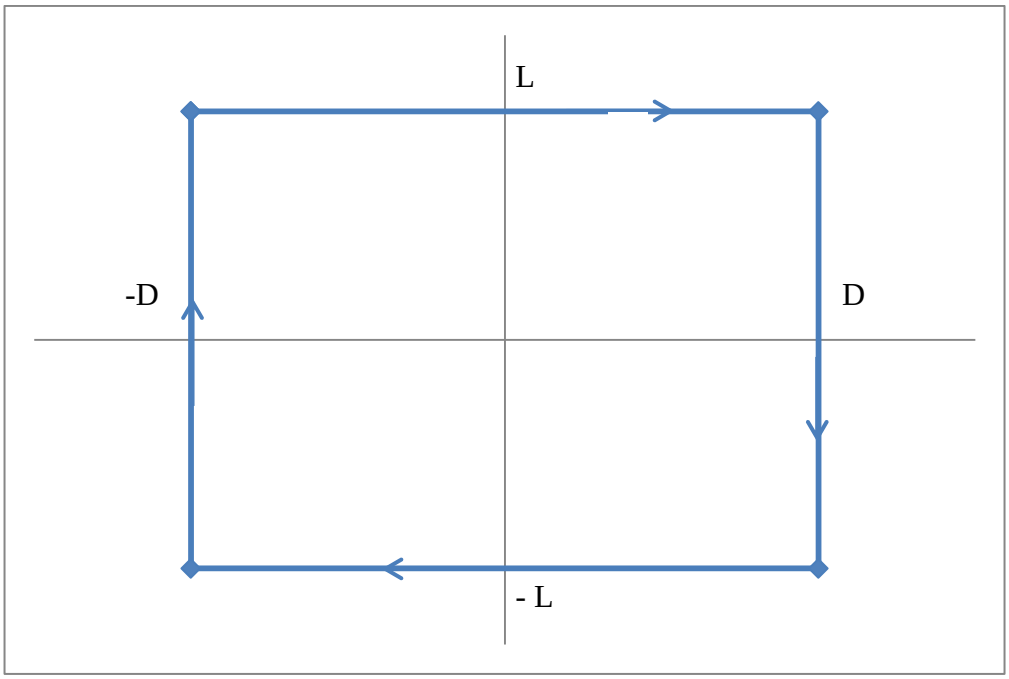

Figure 5.10: Idealized Friction Hysteresis for One Cycle

Toe crushing and splitting of the bricks towards the end of testing also contributed energy dissipation, but the amount is likely much less than the contributions from yielding of the dowels and sliding of the panels on the neoprene pads.

5.6 Summary of Panel Behavior

The two panel specimens both exhibited a rocking response when subjected to lateral loading. By comparing the hysteresis curves obtained during testing (shown in Figures 4.8 and 4.11) with the theoretical bilinear curve depicting rocking behavior (shown in Figure 2.1) it can be seen that the test results largely align with the theoretical response. The differences are due to the energy dissipation resulting in greater area being contained in the hysteresis curves. The energy dissipation is a result of sliding and friction at the neoprene-panel interface and yielding

of the steel dowels. With the engagement of the dowels, a distinct increase in stiffness was seen on the curves.

The following discussion provides a summary of the observed behavior of the panels, particularly with reference to Panel 1 as its response was easier to analyze and understand.

At the beginning of the test, the panel behaved almost elastically, as can be seen during the early cycles in Figures 4.8 and 4.19. Only the friction at the neoprene interface is preventing sliding. At this time, the panel had not started rocking and was oscillating on the neoprene pad. The location of the center of rotation of the panel during testing was located close to the center of the panel for small displacements.

When the lateral displacement exceeds 0.25 in., the foam around the dowels becomes compressed and the dowels are loaded in single shear and act to resist sliding of the panel. This is demonstrated by the sudden increase in load seen in Figure 4.10 indicating a stiffer response. With the sleeve around the top of the dowel allowing vertical motion, the panel starts rocking. It however needs a specific and calculable lateral force to override the amount of axial load. The center of rotation is now located at the interface of the neoprene pad and foam strip. A horizontal plateau characterizing the rocking behavior can be observed in Figures 4.8 and 4.9. The curves are largely bilinear, similar to the theoretical response of a rigid body shown in Figure 2.1. As the rocking increases, a smaller area of neoprene has to carry the axial load. It creates high lateral expansion due to a high Poisson ratio (0.5) and eventually triggers the spalling of the contact bricks due to tension forces.

At a lateral displacement of about 1 in. for Panel 2 and 1.25 in. for Panel 1, the dowels get engaged and stiffen the response of the panel. At the lateral load gets higher, the dowels start yielding in shear, dissipating significant energy. Friction and sliding of the panel at the neoprene

interface is also dissipating energy. This can be seen with the amount of sliding on Figures 4.10 and 4.21. At the same time, uplift results in compression of the foam strips at the toes. As the uplift gets larger, the foam is completely compressed and results in loading at the toes which creates cracks (Panel1) and toe crushing (Panel 2) depending on the amount of axial load.

5.7 Summary and Conclusions

This chapter compared calculated loads to rock the panels and to cause dowel yielding with results obtained from the two panel tests. The performance and effectiveness of the isolation details to produce rocking response and dissipate energy were evaluated. A summary was provided of the observed panel behavior.

Based on equilibrium, the calculated loads to engage rocking of the panels were found to compare well with the rocking loads obtained during testing, especially for Panel 1. Because of the higher axial loads used in Panel 2, rocking behavior began and was quickly followed by the engagement of dowels making comparisons with the calculated rocking loads more difficult.

The shear capacity of the dowels was calculated using the provision given in the MSJC (2011). The resulting shear capacity aligned closely with the second plateau obtained during testing of Panel 1. For Panel 2, the higher axial load resulted in the dowels engaging quickly, complicating evaluation of the behavior for this panel.

The effects of a higher axial load (from 20 kips for Panel 1 to 50 and 40 kips for Panel 2) increases the load at which the rocking plateau occurs and resulted in greater damage to the panel.

Energy dissipation in both specimens was determined using Trapezoidal Rule. Yielding of the dowels contributed significantly to energy dissipation. Friction and sliding of the panel on the

neoprene pad was also a major contributor to energy dissipation. By normalizing the energy dissipation to the axial load, it was seen that axial load strongly influences the amount of energy dissipation. However, lateral expansion of the neoprene created tension forces on the bricks above, resulting in eventual spalling of the bricks. This was particularly evident in Panel 2 with the higher axial loads where spalling occurred on both sides of the wall along the full length of neoprene pad. Other contributions to energy dissipation from cracking and toe crushing were likely modest.

For the panel with lower axial loading, only minor damage developed in the panel even when loaded to 3 in. of lateral displacement, corresponding to a lateral drift of more than 5%. Even in the panel with higher axial loading, significant damage did not develop until the lateral displacements exceeded 1.0 in of lateral displacement, corresponding to a lateral drift of nearly 2%. The special isolation details proposed for the veneer panels were successful in developing the intended rocking response.

CHAPTER 6: SUMMARY, CONCLUSIONS AND RECOMMENDATIONS

6.1 Summary and Conclusions

The objective of this project was to evaluate the effectiveness of special isolation details designed to enable rocking response in masonry veneer panels subjected to lateral displacements. Rocking is expected to reduce or eliminate damage to the masonry panel in a seismic event. Criteria considered in evaluating panel performance the effectiveness of the isolation details included strength, energy dissipation, residual displacement, extent of damage and rocking behavior.

Two masonry veneer panels incorporating the special details were constructed and tested at the Composite Materials and Engineering Center at Washington State University using different axial loads. The panels were nominally 4.5 feet in height and 4 feet in width. The special details incorporated in the panels consist of three elements. First, foam strips were placed at the outer ends of the panels. These strips effectively create a void and are intended to protect the toes of the panel. Second, a neoprene pad was placed at the interface of the panel and the footing covering around 50% of the contact area. The neoprene pad serves to transfer axial loading and to resist shear through friction. Finally, two steel dowels were embedded into the footing and incorporated a bond breaker over the top half of the dowels to allow vertical slip between the dowels and the panel to enable rocking. The dowels also help to re-center the panel after rocking and, at large lateral displacements, resist shear and provide an energy dissipating mechanism once dowel yielding occurs. The dowels were surrounded by foam wrapping at their base to allow approximately 0.25-in. of sliding before the dowels were engaged.

Panel 1 exhibited stable rocking behavior during testing. Very little damage was observed in this specimen. After removal of the panel, bending of the dowels was evident as well as the complete compression of the foam strips. The neoprene pad exhibited no damage. Rocking initiated at 0.5 in. of lateral displacement with the center of rotation located at the interface of the neoprene pad and foam strip, approximately 12 in. from the center of the panel. Two load plateaus were evident in the load-displacement hysteresis curves. The first plateau was at around 5 kips of in-plane load and was a result of rocking of the panel. The second plateau was at around 13 kips and was associated with yielding of the dowels. Panel 1 experienced significant sliding on the footing, with nearly 1 in. of permanent displacement at the end of testing.

Panel 2 also exhibited rocking behavior during testing, but substantial damage occurred to the panel because due to the larger axial loads resulting in a more complex response. Splitting and spalling of the bricks above the neoprene pad on both sides of the panel and significant toe crushing at the South occurred during testing. After removal of the panel from the footing, complete compression of the foam strips was observed similar to that for Panel 1, but the bending of the dowels was more significant. The hysteresis curves were substantially different from those for Panel 1. They were not symmetrical, no clear load plateau could be determined for rocking, and there was a plateau for positive load at around 18 kips near the end of testing. Significant sliding representing half of the input lateral displacements were recorded before the loss of the instrument measuring sliding. The larger axial loads for Panel 2 resulted in increased lateral capacity and stiffness.

Yielding of the dowels contributed significantly to energy dissipation. Friction and sliding of the panel on the neoprene pad was also a major contributor to energy dissipation. By normalizing the energy dissipation to the axial load, it was seen that axial load strongly

influences the amount of energy dissipation. However, lateral expansion of the neoprene created tension forces on the bricks above, resulting in eventual spalling of the bricks. This was particularly evident in Panel 2 with the higher axial loads where spalling occurred on both sides of the panel along the full length of neoprene pad. Other contributions to energy dissipation from cracking and toe crushing were likely modest.

For the panel with lower axial loading, only minor damage developed in the panel even when loaded to 3 in. of lateral displacement, corresponding to a lateral drift of more than 5%. Even in the panel with higher axial loading, significant damage did not develop until the lateral displacements exceeded 1.0 in of lateral displacement, corresponding to a lateral drift of nearly 2%. The special isolation details proposed for the veneer panels were successful in developing the intended rocking response.

6.2 Recommendations and Future Research

The following recommendations are made for possible future research to better understand and potentially improve the rocking response in masonry veneer panels.

It was seen in this study that the center of rotation once rocking initiated was at the neoprene-foam interface. The length of the neoprene pad actually sets the location of the center of rotation and consequently controls the lateral load required to cause rocking. Changing this length would affect the global behavior of the panel. However, sufficient area of neoprene pad to carry the axial load is also a consideration.

The conclusions made in this thesis are limited to the two specimens that were tested. Additional research is recommended to provide additional information on rocking behavior with

these isolation details. Numerical modeling of the panels should also be explored as a way to obtain greater understanding of panel behavior, particularly for larger axial loads.

BIBLIOGRAPHY

Aslam, M., G. Godden, and T. Scalise. "Earthquake rocking response of rigid bodies." *Journal of Structural Engineering (ASCE)*, 1980: 377-392.

Cheng, Chin Tung. "Shaking table tests of a self-centering designed bridge substructure." *Engineering Structures*, 2008: 3426-3433.

Christopoulos, C., A. Filiatrault, and B. Folz. "Seismic Response of Self-Centering Hysteretic SDOF Systems." *Earthquake Engineering and Structural Dynamics*, 2002: 1131-1150.

ElGawady, M. A., Quincy Ma, John Butterworth, and Jason Ingham. "Effects of interface material on the performance of free rocking blocks." *Earthquake Engineering and Structural Dynamics*, 2011: 375-392.

Eurocode, EN8. *Design of Structures for Earthquake Resistance- Part 1: General rules seismic, actions and rules for buildings.* 2009.

"FEMA 306. Evaluation of Eathquake Damaged Concrete and Masonry Wall Buildings." *ATC-43 Project for the Partnership for Response and Recovery*, 1999.

Filiatrault, Andre, Jose Restrepo, and Constantin Christopoulos. "Development of Self-Centering Earthquake Resisting Systems." *13th World Conference on Earthquake Engineering.* Vancouver, B.C. Canada, 2004.

Garcia-Pujador, Rodolfo. *Shaking table study of rocking column bridge based on damage avoidance design.* State University of New York at Buffalo, 1998.

Hitaka, Toko, and Kenji Sakino. "Cyclic tests on a hybrid coupled wall utilizing a rocking mechanism." *Earthquake Engineering and Structural Dynamics*, 2008: 1657-1676.

Holden, T., J. I. Restrepo, and J. B. Mander. "Seismic performance of precast reinforced and prestressed concrete walls." *Journal of Structural Engineering*, 2002: 286-296.

Housner, G. W. "The behavior of inverted pendulum structures during earthquakes." *Bulletin of the Seismological Society of America*, 1963: 403-417.

Kelly, Trevor E. "Tentative Seismic Design Guidelines for Rocking Structures." *Bulletin of New Zealand Society for Earthquake Engineering*, 2009: 239-274.

Kuruma, Y., R. Sause, S. Pessiki, and W. Lu. "Lateral load behavior ans seismic design of unbonded post-tensioned precast concrete walls." *ACI Structural Journal*, 1999: 622-632.

Lipscombe, P. R. *Dynamics of rigid block structures.* Dissertation submitted to the University of Cambridge for the Doctor of Philosophy, 1990.

Mander, J. B., and C. T. Cheng. *Seismic resistance of bridge piers based on damage avoidance design.* State University of New York, Buffalo: Technical Report NCEER-97-0014 (National Center for Earthquake Engineering Research), 1997.

Masonry, Standards Joint Committee(MSJC). *Building Code Requirements for Masonry Structures, 2011.* American Concrete Institute, Farmington Hills, MI., American Sociery of Civil Engineers, Reston, VA., and the Masonry Society, CO.

Meek, J. W. "Effects of Foundation Tipping on Dynamic Response." *Journal Struct. Div. ASCE Vol. 101 No. ST7*, 1978: 1297-1311.

New Zealand Standards. *Code of Practive for General Structural Design and Design Loadings for Buildings, NZS 4203:1992.* 1992.

New Zealand Standards. *Structural Design Actions, Part 5: Earthquake Actions NZS 1170:2004.* 2002.

Pennucci, D., G. M. Calvi, and T. J. Sullivan. "Displacement-based design of precast walls with additional dampers." *Journal of Earthquake Engineering*, 2009: 40-65.

Priestley, M. J. N., R. J. Evison, and A. J. Carr. "Seismic response of sructures free to rock on their foundations." *Bulletin of the New Zealand National Society for Earthquae Engineering*, 1978: 141-150.

Priestley, M. J., and J. R. Tao. "Seismic Response of Prescast Prestressed Concrete frames with Partially Debonded Tendons." *PCI Journal*, January-February 1993: 58-69.

Prieto, Francisco, and Paulo B. Lourenço. "On the rocking behavior of rigid objects." *Meccanica*, 2005: 121-133.

Restrepo, José I., and Amar Rahman. "Seismic Performance of Self-Centering Structural Walls Incorporating Energy Dissipators." *Journal of Structural Engineering*, November 2007: 1560-1570.

Roh, Hwasung, and Andrei Reinhorn. "Nonlinear static analysis of structures with rocking columns." *Journal of Structural Engineering*, 2010: 532-542.

Stanton, J., W. Stone, and G. S. Cheok. "A hybrid reinforced precast frame for seismic regions." *PCI*, 1997: 20-32.

Toranzo, L. A., J. I. Restrepo, J. B. Mander, and A. J. Carr. "Shake-Table Tests of Confined-Masonry Rocking Walls with Supplementary Hysteretic Damping." *Journal of Earthquake Engineering*, 2009.

Toranzo, L. *The use of rocking walls in confined masonry structures: a performance-based approach.* University of Canterbury, New Zealand: PhD Thesis, Department of Civil Engineering, 2002.

Vasconcelos, G., and P. B. Lourenço. "In-plane experimental behavior of stone masonry walls under cyclic loading." *Journal of strutural engineering*, 2009: 1269-1277.